Received: 8 June 2020 | Revised: 15 September 2020 | Accepted: 1 October 2020

DOI: 10.1002/pld3.282

ORIGINAL RESEARCH

Structure-function analysis of the maize bulliform cell cuticle and its potential role in dehydration and leaf rolling

Susanne Matschi[1] | Miguel F. Vasquez[1] | Richard Bourgault[2] | Paul Steinbach[3] | James Chamness[4] | Nicholas Kaczmar[4] | Michael A. Gore[4] | Isabel Molina[2] | Laurie G. Smith[1]

[1]Section of Cell and Developmental Biology, University of California San Diego, La Jolla, CA, USA

[2]Department of Biology, Algoma University, Sault Ste. Marie, ON, Canada

[3]Howard Hughes Medical Institute, University of California San Diego, La Jolla, CA, USA

[4]Plant Breeding and Genetics Section, School of Integrative Plant Science, Cornell University, Ithaca, NY, USA

Correspondence
Laurie G. Smith, Section of Cell and Developmental Biology, University of California San Diego, La Jolla, CA 92093, USA.
Email: lgsmith@ucsd.edu

Present address
Susanne Matschi, Department Biochemistry of Plant Interactions, Leibniz Institute of Plant Biochemistry, Weinberg 3, Halle (Saale), Germany
James Chamness, Department of Genetics, Cell Biology, and Development, University of Minnesota, Saint Paul, MN 55108, USA

Funding information
NSF | BIO | Division of Integrative Organismal Systems (IOS), Grant/Award Number: IOS1444507; Deutsche Forschungsgemeinschaft (DFG), Grant/Award Number: MA-7608/1-1; Canada Research Chairs (Chaires de recherche du Canada)

Abstract

The hydrophobic cuticle of plant shoots serves as an important interaction interface with the environment. It consists of the lipid polymer cutin, embedded with and covered by waxes, and provides protection against stresses including desiccation, UV radiation, and pathogen attack. Bulliform cells form in longitudinal strips on the adaxial leaf surface, and have been implicated in the leaf rolling response observed in drought-stressed grass leaves. In this study, we show that bulliform cells of the adult maize leaf epidermis have a specialized cuticle, and we investigate its function along with that of bulliform cells themselves. Bulliform cells displayed increased shrinkage compared to other epidermal cell types during dehydration of the leaf, providing a potential mechanism to facilitate leaf rolling. Analysis of natural variation was used to relate bulliform strip patterning to leaf rolling rate, providing further evidence of a role for bulliform cells in leaf rolling. Bulliform cell cuticles showed a distinct ultrastructure with increased cuticle thickness compared to other leaf epidermal cells. Comparisons of cuticular conductance between adaxial and abaxial leaf surfaces, and between bulliform-enriched mutants versus wild-type siblings, showed a correlation between elevated water loss rates and presence or increased density of bulliform cells, suggesting that bulliform cuticles are more water-permeable. Biochemical analysis revealed altered cutin composition and increased cutin monomer content in bulliform-enriched tissues. In particular, our findings suggest that an increase in 9,10-epoxy-18-hydroxyoctadecanoic acid content, and a lower proportion of ferulate, are characteristics of bulliform cuticles. We hypothesize that elevated water permeability of the bulliform cell cuticle contributes to the differential shrinkage of these cells during leaf dehydration, thereby facilitating the function of bulliform cells in stress-induced leaf rolling observed in grasses.

KEYWORDS
bulliform cells, cuticle, drought/water stress, leaf rolling, lipid metabolism, maize, ultrastructure

1 | INTRODUCTION

Plants display a variety of responses to environmental stresses. An important drought stress response in grasses is reversible leaf rolling along the longitudinal leaf axis upon water limitation or heat stress conditions. Leaf rolling prevents water loss, photosynthetic loss, and increases drought resistance in numerous species of the Poaceae (Kadioglu & Terzi, 2007; Saglam et al., 2014), which include staple crops like wheat, rice, and maize. Dehydrated grass leaf blades fold longitudinally, reducing the exposed leaf surface area, with effects on leaf transpiration and canopy temperature (O'Toole et al., 1979; Turner et al., 1986). Leaf rolling is linked to osmotic adjustment and a change in leaf water potential upon dehydration (Hsiao et al., 1984; Moulia, 1994; O'Toole & Cruz, 1980). Changes in concentrations of organic acids or ions, accumulation of phytohormones, in part followed by changes in stress-responsive gene expression, and other abiotic and biotic factors contribute to leaf-rolling (Kadioglu et al., 2012).

Bulliform cells (BCs) are enlarged, colorless cells located in the epidermis, which in maize are usually arranged in 2 to 5 cell-wide strips along the longitudinal leaf axis solely on the adaxial side of the leaf (Becraft et al., 2002; Ellis, 1976; Sylvester & Smith, 2009). Being absent in juvenile maize leaves, their emergence in the leaf epidermis is one of the hallmarks of the vegetative phase change in maize, the transition from juvenile to adult leaves (Poethig, 1990). The function of BCs, also called hinge or motor cells, is a matter of ongoing debate since the first description by Duval-Jouve (1875) postulating reversible rolling of the leaf blade resulting from changes in the turgor pressures of BCs. Adaxial rolling is conferred by differential top–bottom elastic shrinkage in the leaf cross-section (Moulia, 2000) which is thought to be guided by BCs due to their asymmetric location on the adaxial leaf surface. However, studies on leaf rolling in different grass types reach contradictory conclusions and could not resolve whether BCs cause rolling by collapse due to water loss, or whether their size and plasticity merely permit them to be compressed and allow rolling to occur (reviewed in Ellis, 1976; Evert, 2006; Moulia, 2000). Nevertheless, numerous mutants with altered BC number, size or adaxial/abaxial patterning, mostly identified in rice (Zou et al., 2014, reviewed in Xu et al., 2018) along with a few in maize (Gao et al., 2019; Nelson et al., 2002), show an effect on leaf rolling and underline the importance of this cell type and its distribution for the leaf rolling response in grasses. Only recently the genetic diversity of maize in combination with association mapping and machine learning techniques was employed to characterize the genetic basis of bulliform strip architecture, namely strip number and width, in a collection of diverse maize inbred lines, and identify a number of underlying candidate genes (Qiao et al., 2019).

The cuticle is the first layer of protection of aerial plant tissue and represents an important interaction surface with the environment. It shields the underlying tissue against environmental stresses such as non-stomatal water loss (Riederer & Schreiber, 1995), UV radiation (Krauss et al., 1997) and pathogen attack (Serrano et al., 2014), which in turn can affect cuticle biogenesis (Yeats & Rose, 2013). The biological functions of cuticles are determined by their physical properties, which depend on their chemical composition. The cuticle is comprised of two major components: the polyester cutin, which serves as the cuticle's framework (Fich et al., 2016), and cuticular waxes, a multitude of mainly hydrophobic compounds that are either embedded into the cutin polymer matrix (intracuticular waxes) or cover the cutin layer (epicuticular waxes) (Koch & Ensikat, 2008). Cutin polymer structures in different species and tissues remain elusive so far, as biochemical characterization of cutin can only be achieved by a description of its monomers after depolymerization. Typical cutin monomers are long-chain (C_{16} and C_{18}) fatty acid (FA) monomers that have a hydroxy group at the ϖ-position and mid-chain hydroxy or epoxy groups. Additionally, unsubstituted fatty acids, dicarboxylic acids (DCA), glycerol, and low amounts of phenolic compounds (e.g. hydroxycinnamic acids (HCAs) like coumarate and ferulate) can be present (Pollard et al., 2008). Cuticular waxes are derived from very long-chain fatty acids (VLCFAs), and usually consist of aldehydes, primary and secondary alcohols, hydrocarbons, ketones, wax esters, and cyclic compounds including terpenoids and sterols (Yeats & Rose, 2013). Unlike cutin, waxes can be extracted from the cuticle with organic solvents.

The cuticle is generally described as having three layers of overlapping composition: (a) the innermost cuticular layer, continuous with the cell wall, which consists of polysaccharides, waxes and cutin; (b) the cuticle proper as the middle layer, with intracuticular waxes embedded in the cutin matrix but devoid of polysaccharides; (c) the epicuticular wax layer as the outermost layer of the cuticle on the plant surface, which may be deposited as an amorphous film or in the form of epicuticular wax crystals (Bargel et al., 2006; Jeffree, 2006). However, recent reassessments of the literature and emerging techniques challenge the concept of the cuticle as a lipid layer independent from the cell wall with very defined structural elements (Fernández et al., 2016), and instead describe the cuticle as a form of lipidic modification of the cell wall (Yeats & Rose, 2013). The thickness, structure and chemical composition of cuticles vary widely between different organisms, developmental stages, and even organs within a species (Jeffree, 2006; Jetter et al., 2006). Understanding how the features of cuticle organization are related to its composition and function is an active area of research.

Retaining water in the epidermis and the underlying plant tissue to limit dehydration is one of the most important roles of the plant cuticle. It is well-known that waxes, rather than cutin, provide the majority of the water barrier property of the cuticle (Isaacson et al., 2009; Jetter & Riederer, 2016; Kerstiens, 1996; Schönherr, 1976). Interestingly, cuticle thickness is no indicator of its effectiveness as a water barrier, but wax composition appears to be critical (Buschhaus & Jetter, 2012; Jetter & Riederer, 2016). In a direct comparison of cuticle permeability in several Arabidopsis mutants with either increased or decreased wax and/or cutin loads, most mutants displayed higher permeability than wild-type, even if their respective wax or cutin load was increased or showed a thicker cuticle (Sadler et al., 2016). Increased wax load in cutin mutants is often interpreted as a compensatory mechanism to ensure cuticular

integrity despite the insufficient cutin scaffold provided in these mutant backgrounds (Bessire et al., 2007; Kurdyukov et al., 2006).

The great majority of cuticle studies in maize focus on juvenile leaves, which are, in addition to other distinctive features, quite different in cuticle structure and composition compared to adult leaves (Bianchi & Marchesi, 1960; Bianchi & Avato, 1984; Bongard-Pierce et al., 1996). Only limited research is available on cuticle composition and function in adult maize leaves, despite the fact that many cuticle-dependent traits are more critical at the adult stage of plant life. For example, drought is most damaging to maize grain yield at the flowering stage (Grant et al., 1989), a time when juvenile leaves have died and only adult leaves remain. The wax profile of the adult leaf cuticle reveals high proportions of wax esters and alkanes and low abundance of free alcohols and aldehydes (Bianchi & Avato, 1984; Bourgault et al., 2020). The cutin polyester in the adult maize leaf mainly consists of di-hydroxy-hexadecanoic acid and typical members of the C_{18} family of cutin acids, including hydroxy and hydroxy-epoxy acids, with low amounts of the HCA derivatives coumarate and ferulate also present (Bourgault et al., 2020; Espelie & Kolattukudy, 1979). In a developmental analysis of the maize leaf cuticle, establishment of the water barrier properties of the adult leaf cuticle coincided with a switch from alkanes to esters as the major wax type and the emergence of an osmiophilic (likely cutin-rich) layer of the cuticle proper (Bourgault et al., 2020). Ultrastructurally, pavement cell cuticles of the adult leaf did not show a typical three-layered composition, consisting only of a cuticle proper and an epicuticular layer (Bourgault et al., 2020).

Little is known about variation in cuticle composition and structure on specific epidermal cell types and how this relates to their specialized functions. This is challenging to investigate due to the difficulty of separating different epidermal cell types for biochemical analysis of cuticle composition. One example of a comparative study was conducted on trichome cuticles in Arabidopsis (Hegebarth et al., 2016), where comparison of trichome-enriched and depleted genotypes revealed an increase in longer chain alkanes and alkenes in trichome-rich material. Integration of gene expression data lead to the conclusion that trichomes possess autonomous wax biosynthesis (Hegebarth et al., 2016; Hegebarth & Jetter, 2017). The exposed position of trichomes requires increased flexibility to withstand mechanical stress, but the role of the trichome cuticle, and its specific composition, is unclear (Hegebarth & Jetter, 2017). Furthermore, there is indirect evidence that the cuticles of guard cells have a different composition compared to those of pavement cells but these differences have yet to be characterized (Hegebarth & Jetter, 2017).

The current study aimed to (a) examine the role of BCs in the adult maize leaf rolling response to dehydration; (b) analyze the structure, composition, and function of BC cuticles; and (c) consider the functional significance of BC cuticles for their proposed function in leaf rolling. To that end, a new cryo-confocal microscopy method was used to demonstrate differential shrinkage, upon leaf dehydration, of BCs relative to other epidermal cells types. Maize's genetic diversity was surveyed to demonstrate a relationship between bulliform strip width and spacing, and leaf rolling speed in excised leaves. Light and electron microscopy were used to define unique features of the bulliform cuticle. To investigate the composition and function of the bulliform cuticle, bulliform-enriched or -depleted tissues were compared with respect to cutin and wax composition as well as cuticular conductance. Transcriptional analysis of the maize leaf cuticle maturation zone of bulliform-enriched mutants was carried out to identify genes that may play important roles in bulliform cuticle formation. Together, our findings add to the scarce knowledge about cell type-specific cuticles, and how structural and compositional cuticle features could relate to the biological function of a specific cell type.

2 | MATERIAL AND METHODS

2.1 | Plant material and growth conditions

Maize inbred B73 was used for experiments unless otherwise stated. All mutants analyzed were introgressed into the B73 background. *wty2* seeds were obtained from Prof. Anne Sylvester (University of Wyoming), *dek1-D* seeds from Prof. Phil Becraft (Iowa State University), and *Xcl1* seeds from Prof. Neelima Sinha (UC Davis). Plant materials and experimental field designs for the leaf rolling analysis have been described previously (Lin et al., 2020; Qiao et al., 2019). For histological, biochemical, and functional analyses, plants were grown in 8-inch pots in a glasshouse on the UCSD campus in La Jolla, CA (latitude 32.8856, longitude −117.2297), without supplementary lighting or humidity control, and with temperatures in the range of 18–30°C. All experiments presented focused on fully expanded adult leaves before or during the flowering stage, starting with the first fully adult leaf (#8 in B73) or concentrating on the leaf subtending the uppermost ear, or one leaf above or below.

2.2 | Cuticular conductance

Cuticular conductance was determined as described previously (Lin et al., 2020). In short, whole adult leaves (3–5 per genotype) were cut 2.5 cm below the ligule and incubated in a dark, well-ventilated room for 2 hr at 20–22°C and 55%–65% RH, with cut ends immersed in water for stomatal closure and full hydration (porometer studies established that 2 hr was more than sufficient to reach g_{min} indicating stomatal closure; Lin et al., 2020). After removal of excess water on the leaf blades, leaves were hung to dry in the same dark, temperature-and humidity-controlled room. To determine g_c, wet weight of each leaf was recorded every 45– 0 min over a time period of 270–300 min, for a total of five or six measurements per leaf. Leaf dry weight was acquired after 4 days of incubation at 60°C in a forced-air oven. Dry weight was shown to be a reasonable approximation of leaf surface area for normalization of g_c (Lin et al., 2020), and was used in the calculation of adult leaf cuticular conductance as follows (g_c): g_c (g/h*g) = −b/ dry weight, where b (g/h) is the coefficient of the linear regression of leaf wet weight (g) on time (h), and

dry weight (g) is an approximation of leaf surface area. In case of petroleum jelly treatment of adaxial or abaxial leaf surfaces, weight loss over time was normalized to starting weight since complete drying of petroleum jelly-treated leaves was not possible.

2.3 | Leaf rolling analysis

Leaf rolling was scored on a set of 468 maize inbred lines from the Wisconsin Diversity panel (Hansey et al., 2011), which at the same time was evaluated for genetic variation of bulliform patterning (Qiao et al., 2019) and leaf cuticular conductance (g_c) of adult maize leaves (Lin et al., 2020). Data on leaf rolling (Table S1) were collected during the phenotypic evaluation of g_c in 2016 at the Maricopa Agricultural Center, Maricopa, AZ. Leaf rolling was recorded during each weight recording for g_c analysis, in 45 min intervals at six time points (TPs) over a span of 270 min, using a visual scale of 0 = not rolled, and 1 = rolled. Our score 1 corresponded to score 5 of fully rolled leaves according to Moulia (1994) (with maize belonging to rolling type 2), while score 0 (not rolled) corresponded to scores 1–4 in Moulia's scoring scale. The TP when leaves were scored to be rolling for the first time (TP1 corresponding to 45 min of dehydration, TP6 corresponding to 270 min), were extracted for each inbred, while leaves which were scored to be unrolled at TP6 got assigned the hypothetical rolling time point TP7 as the most conservative estimation. Pearson's correlations between bulliform patterning (number and width of BC strips, Table S1, extracted BLUPs for the Maricopa/AZ environment from Qiao et al., 2019) and leaf rolling data were analyzed for 291 inbreds in total (overlap between datasets of 316 lines with data for leaf rolling and dataset of 410 lines with data for bulliform patterning). Lines with extreme rolling behavior—"fast rollers" (rolled within the first 90 min of dehydration, 25 lines), and "never rollers" (no rolling observed in the assessed time frame, 38 lines)—were grouped and additionally graphed independently.

2.4 | Cryo-microscopy of dehydrated leaves

Adult B73 leaves were cut below the ligule and hung to dry in the dark for 4 hr, while control leaves were kept hydrated by submerging the cut end in water. Immediately after, blade tissue from the midsection of the leaves was cut, submerged in cryomolds containing room-temperature optimal cutting temperature compound (OCT, Sakura Finetek USA) and frozen in liquid nitrogen. The frozen OCT blocks were milled flat using a Leica CM 1950 cyrostat, exposing the leaf tissue remaining in the block at the biologically relevant level while discarding the remnants of the cryosections. The frozen block face with the exposed, intact leaf tissue was transferred to a Nikon A1plus Eclipse Ni-E confocal microscope, equipped with a liquid nitrogen-cooled imaging chamber custom-built by Paul Steinbach (laboratory of Dr. Roger Tsien, UCSD), designed to maintain the frozen samples at ~40°C, and imaged directly with the confocal microscope with a 4X (NA 2.0) objective. Autofluorescence of plant tissue was detected with excitation at 405 nm and emission detection at 525 nm. Cell size measurements were done with ImageJ (v1.50i, https://imagej.nih.gov/ij/).

2.5 | TEM and other Imaging

TEM sample preparation and imaging were done as previously described (Bourgault et al., 2020). Glue impressions of adult maize leaves were collected as described previously (Qiao et al., 2019). For examples of natural variation of bulliform strip patterning in Figure 1a-d, impressions of different inbreds were imaged with a Nikon SMZ-U Stereoscopic Zoom Microscope, using a 0.5 objective lens with a Lumenera InfinityX camera attached. For analysis of cuticular nanoridges and adaxial hair type quantification, glue impressions of bulliform mutants were imaged with a Keyence VHX-6000 digital microscope, equipped with a VH-ZST lens. Hand cross-sections of adult leaf blade material of bulliform mutants were imaged on a Nikon Eclipse E600 Microscope with a Lumenera InfinityX camera attached.

2.6 | Fluorol Yellow staining

Tissue samples of the middle section of adult leaves were collected and fixed in Formalin-Acid-Alcohol (ethanol (>90%) 50%, glacial acetic acid 5%, formalin (37% formaldehyde) 10%). Fixed samples were infiltrated in gradual increases to 30% sucrose solution, embedded in OCT compound (Sakura Finetek USA) and frozen into cryoblocks. 20 μm block face sections were collected on 1% polyethylenimine (PEI) coated slides, stained with 0.1% calcofluor white (aq., Sigma Aldrich) for five minutes followed by 0.01% Fluorol Yellow (Santa Cruz Biotechnology) in lactic acid solution for 30 min, mounted in Vectashield anti-fade mounting medium (VECTOR Laboratories), and sealed underneath a coverslip by nail polish. Images were captured on a Zeiss LSM 880 Confocal with FAST Airyscan using Plan-Apochromat 10X/0.45 M27, Plan-Apochromat 20x/0.8 M27, Plan-Apochromat 63x/1.4 Oil DIC M27 objectives set at 515 nm emission/488 nm excitation wavelength for Fluorol Yellow and 450 nm emission/405 nm excitation wavelength for calcofluor white. Collected images were processed through superresolution Airyscan and composite pictures were processed through ImageJ. Cell counts of epidermal cell types were done with ImageJ.

2.7 | Analysis of leaf cuticular lipids

Abaxial and adaxial B73 cuticles: Adaxial and abaxial leaf surfaces were used from the portion between 20 and 42 cm of maize B73 partially expanded leaf #8 after removing the midrib. Total waxes were extracted following the method described in Buschhaus et al. (2007) with some modifications. A 25 ml glass tube containing 8 ml chloroform was placed against the leaf surface held to the rim

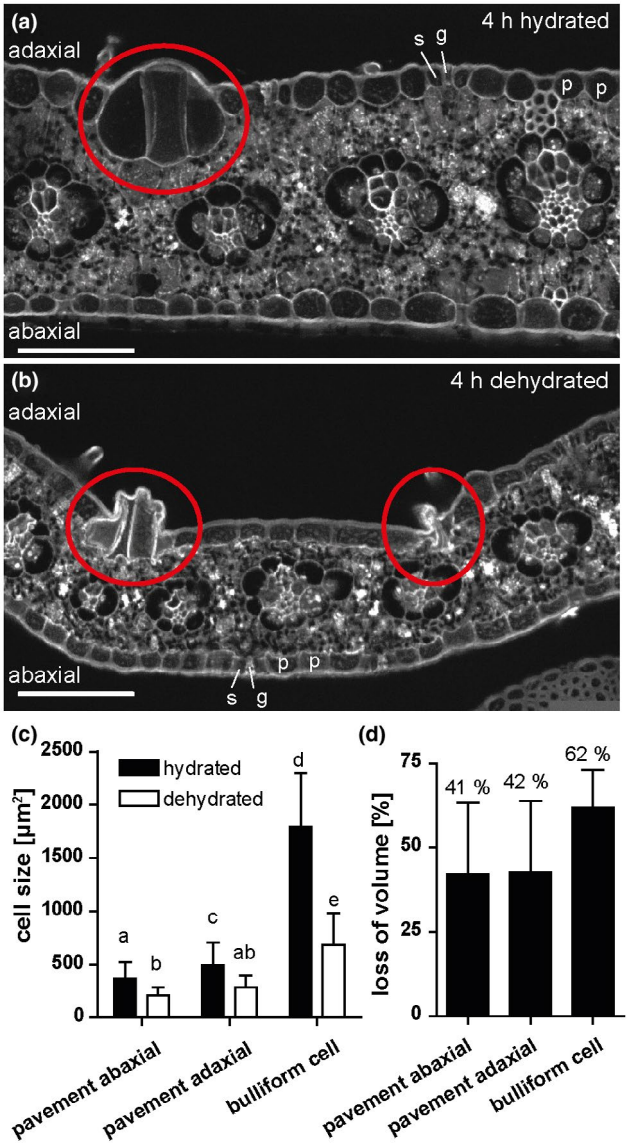

FIGURE 1 Bulliform cells show increased shrinkage upon dehydration. (a-b) Cross-sections of (de-)hydrated maize leaf tissue after 4 hr in the dark. Tissue was shock-frozen after 4 hr without fixation, and autofluorescence was detected by in situ-cryo-imaging as described in Methods. p = pavement cell, g = guard cell, s = subsidiary cell, red circle = group of bulliform cells. Scale bar = 100 µm. (c) Cell sizes (cross-sectional areas) of the indicated epidermal cell types, analyzed by ImageJ. (d) Quantification of cell shrinkage of different cell types upon dehydration as loss of volume in percentage. Shrunken bulliform cells were counted only if their outlines could be seen as in the group on the left in B (i.e. severely shrunken bulliform groups such as the one on the right in (b) were not counted). Values given as means + *SD* (n = 88–194 cells per cell type). Statistical analysis used 1-way ANOVA, means with the same letter are not significantly different from each other; Tukey's post-test, $p < .05$

of the tube using mild thumb pressure. The chloroform was shaken against the surface of the leaf for 30 s. This was repeated along the entire 22 cm length of the leaf and each leaf-half was used for either abaxial or adaxial extraction. Internal standards were added to the extracts; 1.5 µg of each, n-tetracosane, 1-pentadecanol, and heptadecanoic acid. Extracts were dried under a nitrogen stream and analyzed as described in Bourgault et al. (2020). To determine cutin monomer composition of adaxial and abaxial leaf surfaces, cuticles were isolated from the same portion of B73 leaves described above, using enzymatic digestion (Bourgault et al., 2020). Isolated cuticles were delipidated and dried under a nitrogen stream. Dry weight was recorded at this stage and 10 µg internal standards were added to all extracts; pentadecanolactone and methyl heptadecanoic acid. Samples were then depolymerized and the released monomers were analyzed by GC-MS as described in Bourgault et al. (2020).

Bulliform mutant cuticles: Total waxes were extracted by chloroform immersion from bulliform-overproducing mutants (*wty2*, *dek1-D*, and *Xcl1*) and their respective wild-type siblings using expanded segments of adult leaves. Tissues remaining after chloroform extraction were delipidated and chemically depolymerized. Both wax extracts and cutin monomers were transformed into their TMSi derivatives and analyzed by GC-MS and GC-FID following the same procedures described in Bourgault et al. (2020).

2.8 | RNAseq analysis

Total plant RNA of developing adult leaves (10%–30% of leaf length of the maturing leaf at 50 to 60 cm, where cuticle maturation is most prominent according to Bourgault et al., 2020) was isolated with the RNeasy Plant Mini Kit (Qiagen) according to the manufacturer's instructions. Library preparation and RNAseq were performed by Novogene. Sequencing libraries were generated using the NEBNext® Ultra™ RNA Library Prep Kit for Illumina (NEB). Clustering of index-coded samples was performed on a cBot Cluster Generation System using TruSeq PE Cluster Kit v3-cBot-HS (Illumina). Sequencing was carried out on an Illumina platform, and paired-end reads were generated. The filtered reads were aligned to the most recent version of the maize reference genome, B73_v4 (release-44), using HISAT2 (version 2.1.0, Kim et al., 2015). HTSeq v0.6.1 (Anders et al., 2015) was used to count the reads numbers mapped to each gene, and the Fragments Per Kilobase of transcript sequence per Million base pairs sequenced (FPKM) of each gene was calculated based on the length of the gene and reads count mapped to this gene. Differential expression analysis was performed using the DESeq R package (1.18.0, Anders & Huber, 2010), and p-values were adjusted using the Benjamini and Hochberg's approach. Amino acid sequences of maize candidate genes were compared to Arabidopsis protein sequences using the BLAST tool (Altschul et al., 1997) on the TAIR website (https://www.arabidopsis.org).

2.9 | Data availability and statistical analysis

The raw RNAseq data are deposited at NCBI SRA with the BioProject ID PRJNA605434. Statistically significant differences for all experiments were determined by the statistical tests referred to in Figure legends using GraphPadPrism (version 4; GraphPad Software).

3 | RESULTS

3.1 | Bulliform cells display differential shrinkage upon dehydration

Disproportionate shrinkage of bulliform cells (BCs), located only on the adaxial side of the leaf, during leaf dehydration is thought to create a hinge-like effect promoting leaf rolling. However, we could not find published experimental evidence confirming this hypothesis. Indeed, it is technically challenging to investigate this, since conventional methods permitting visualization of plant tissues at the cellular level have the potential to cause cell shrinkage in their own right (e.g. fixation and dehydration prior to embedding in a sectioning medium), or reverse cell shrinkage (e.g. if freshly cut hand sections of dehydrated tissue are mounted in aqueous medium under a cover slip). To overcome these problems, a newly established cryo-confocal imaging method was employed. After 4 hr of dehydration of detached, but intact, adult leaves (or no dehydration), tissue fragments were shock-frozen in optimal cutting temperature compound (OCT) and cross-sectioned in a cryo-microtome. Autofluorescence of tissue cross-sections exposed at the block face was then imaged in a custom-built liquid N_2-cooled chamber mounted on a confocal microscope (Figure 1). In comparison with cross-sections of fully hydrated control leaves (Figure 1a), pavement cells as well as bulliform cells (red circles) were smaller in dehydrated (rolled) leaves (Figure 1b). Bulliform cells shrank more than pavement cells (Figure 1c,d), but no difference in shrinkage was observed comparing adaxial and abaxial pavement cells. These results show in situ that BCs shrink differentially during leaf dehydration, supporting a role for this cell type in driving leaf rolling.

3.2 | Maize leaf rolling is impacted by variation in bulliform strip patterning

BCs are organized into 2–5 cell wide strips aligned with the proximodistal axis of the maize leaf. Phenotypic diversity in a panel of diverse maize inbred lines was used to query the relationship between BC patterning and the leaf rolling response to dehydration. Adult leaves of maize inbred lines differ considerably in the frequency and width of bulliform strips (examples in Figure 2a-d). In addition to BC patterns (Qiao et al., 2019), leaf rolling responses during dehydration were recorded for each of several hundred different maize inbred lines. Adult leaves were excised from each plant, hung from a line to allow them to dehydrate, and scored for their leaf rolling status as a function of time (Figure 2e, Table S1). Lines with extreme rolling behavior- "fast rolling" (scored as rolled within the first 90 min of dehydration, 25 lines), and "never rolling" (no rolling observed in the assessed time frame of 270 min, 38 lines)—were selected for analysis. Rolling behavior in these lines was significantly related to the pattern of BC strips (Figure 2f-h). Fast-rolling leaves had a higher number of BC strips per unit area than never-rolling leaves (Figure 2f), while the width of individual bulliform strips showed the inverse trend, with never-rolling leaves exhibiting wider strips than fast-rolling leaves (Figure 2g). However, overall bulliform coverage was not different between fast- and never-rollers (Figure 2h). Bulliform strip number and width appear to impact leaf rolling independently, since no correlation was seen between these features across the entire set of inbred lines studied (Figure S1). While other (unknown) phenotypic differences between these genetically diverse lines presumably explain most of the difference in rolling rate between fast-rollers and never-rollers, our finding of a significant relationship between rolling rate and bulliform strip patterns further supports a role for BCs in the leaf rolling response, and suggests that rolling is facilitated by more closely spaced and narrower bulliform strips.

3.3 | Pavement and bulliform cell cuticles of the adult maize leaf have distinct ultrastructure

Since cuticles play a role in protecting cells of the shoot against water loss, we compared cuticles of bulliform versus pavement cells of adult, fully mature maize leaves via transmission electron microscopy (TEM) and confocal microscopy (Figure 3). As previously described, TEM reveals that pavement cells have a thin cuticle with four ultrastructurally defined zones of distinct osmium staining characteristics (Figure 3a,b; Bourgault et al., 2020). Epicuticular wax forms an outer, dark-staining layer, while the innermost, dark-staining layer could reflect the pectin-rich wall/cuticle interface described for many other plant species (Jeffree, 2006). Between these two layers, dark- and light-staining layers can be observed; these were classified previously as distinct zones of the cuticle proper (Bourgault et al., 2020), since both layers are missing the polysaccharide fibrils characteristic of a cuticular layer. Cuticles of bulliform cells (Figure 3c) are strikingly different from those of pavement cells: they are fourfold thicker (Figure 3d), and exhibit a different organization. The epicuticular wax layer of BCs is comparable, but the cell wall/cuticle interface is diffuse compared to a pavement cell. Dark-staining fibrils are seen reaching into the cuticle from the cuticle-wall interface, mostly aligned perpendicular to the plane of the cuticle; these are characteristic of a cuticular layer with polysaccharides embedded (Jeffree, 2006; Mazurek et al., 2017). A layer devoid of these fibrils (cuticle proper) can be seen directly underneath the epicuticular wax layer, but lacks distinct dark and light-staining zones seen in pavement cell cuticles. Therefore, BC cuticles exhibit a standard cuticle consisting of a cuticular layer, cuticle proper and epicuticular wax layer (Jeffree, 2006). A difference between pavement and BC cuticles was also apparent in leaf cross sections stained with Fluorol yellow 088 (FY) and imaged via confocal microscopy (Figure 3e,f). Whereas pavement cells showed very thin or no FY staining, BCs displayed bright FY staining. A clear, immediate decrease in cuticle thickness (FY staining) can be observed at the boundary between bulliform and pavement cells, where BC and pavement (P) cell walls meet (stained by Calcofluor white, CW; Figure 3f). In summary, compared to pavement cells, BCs have much thicker cuticle with a prominent cuticular layer.

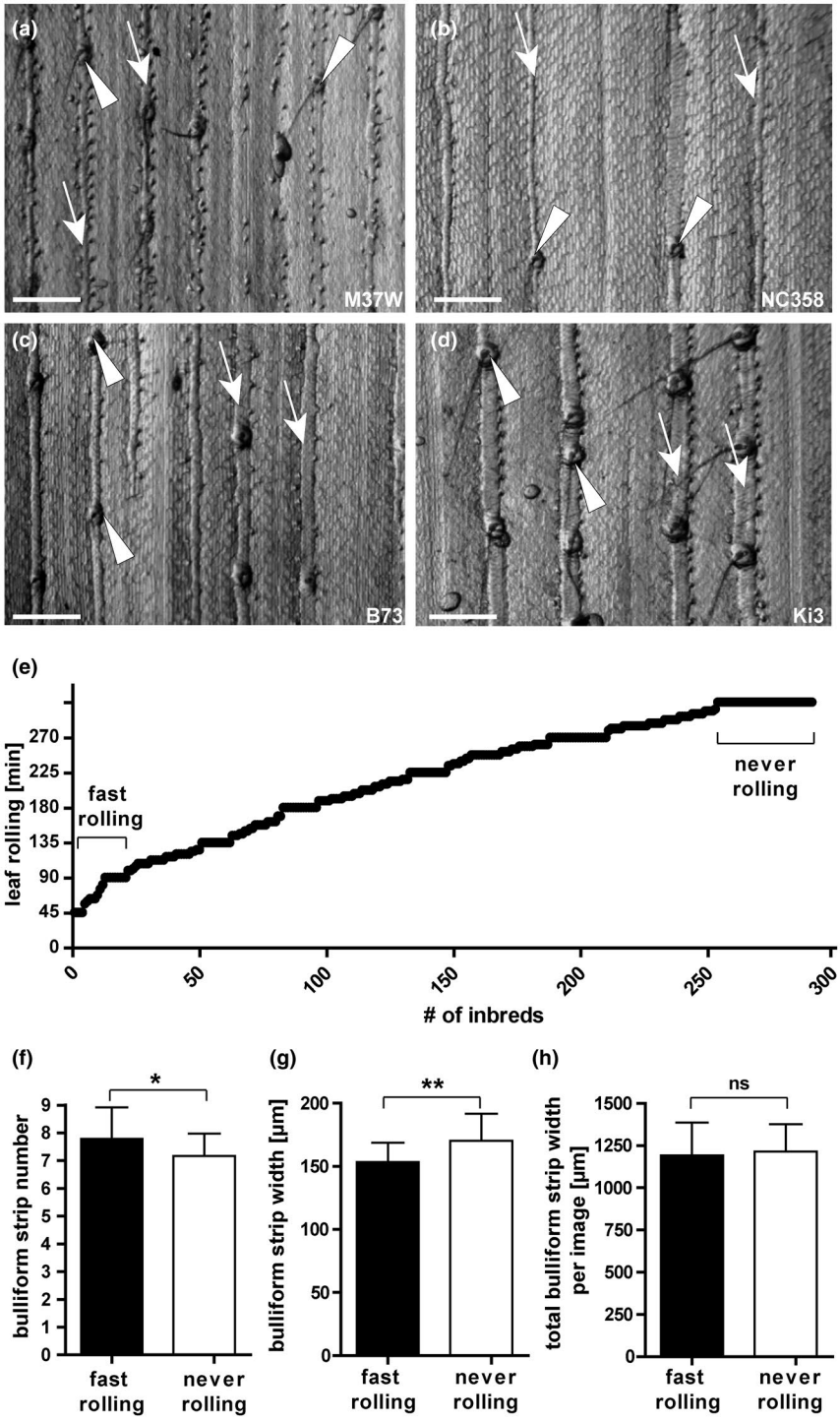

FIGURE 2 Bulliform patterning correlates with leaf rolling speed. (a-d) Grayscale images of leaf epidermal glue-impressions from four maize inbred lines showing divergent bulliform cell patterning phenotypes: M37W and NC358 have narrow bulliform strips, while B73 and Ki3 have wide strips; M37W and B73 have closely spaced strips (7 per field of view), while NC358 and Ki3 have widely-spaced strips (4 per field). Arrow = single bulliform strip, arrowhead = macrohair. Scale bar = 500 µm. (e) Distribution of leaf rolling speeds in minutes shown on Y-axis, after onset of dehydration when 50% rolled status was observed, for 291 inbreds of the WiDiv collection (data can be found in Table S1). Fast- and never-rolling lines used for analysis in F-H are highlighted. (f-h) Comparison of bulliform strip number per field of view at standard magnification (f), individual strip width (g), and total bulliform strip width per image (strip number x width) (h). Means in (f-h) are compared for 25 fast-rolling maize inbreds (rolled within 90 min) and 38 never-rolling inbreds (not rolled within 270 min of dehydration), assessed in a detached leaf dehydration assay in the dark in controlled conditions of 20–22°C and 55%–65% humidity. Values are given as means + standard deviation (*SD*), statistical analysis used two-tailed unpaired Student's t-test, with $^{*}p < .05$, $^{**}p < .01$

3.4 | Bulliform-enriched tissue shows increased epidermal water loss upon dehydration

To investigate the functional significance of the observed differences between BC and pavement cell cuticles, we utilized mutants enriched in bulliform-like cells. Three different maize mutant lines with previously described epidermal aberrations on adult leaves were identified and analyzed. The *warty2* (*wty2*) mutant is defective in a tyrosine kinase gene (Luo et al., 2013) and shows, similar to *wty1* (Reynolds et al., 1998; Sylvester & Smith, 2009), disordered cell expansion in the leaf blade producing large patches of overly expanded, BC-like epidermal cells ("warts") on both sides of the leaf (Figure 4a,b). Mutants homozygous for a weak allele of *defective kernel1* called *dek1-Dooner* (*dek1-D*), a mutation in a gene encoding a plasma-membrane protein with 21 transmembrane domains and a calpain protease domain, display an increased frequency of bulliform-like cells on both abaxial and adaxial surfaces (Figure 4c) (Becraft et al., 2002). The *extra cell layers1* (*Xcl1*) mutant, with a semi-dominant mutation in an unknown gene, causes extra cell layers with epidermal characteristics, previously described as similar to

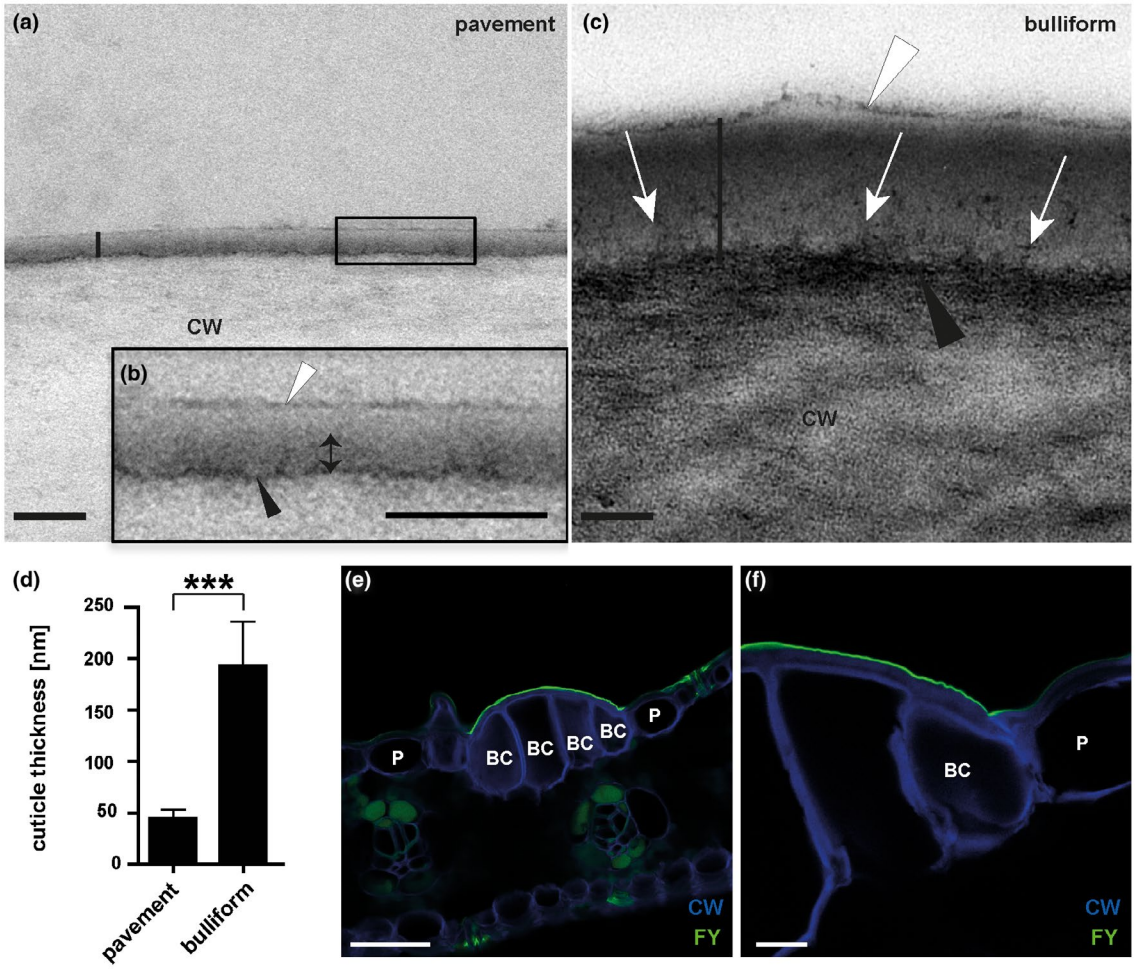

FIGURE 3 Bulliform and pavement cell cuticles have different thicknesses and ultrastructures. (a-b) Pavement cell cuticle from a fully expanded adult maize leaf, visualized by TEM (vertical black line marks the full extent of the cuticle), where (b) is the magnified version of the black box in A. Four distinct layers or zones are visible: a thin, darkly stained layer (black arrowhead) at the interface between the cell wall (CW) and cuticle, dark (double headed arrow) and light zones of the cuticle proper, and a darkly stained epicuticular layer (white arrowhead). (c) Bulliform cell cuticle, visualized by TEM (extent marked by vertical black line). The cell wall/cuticle interface (black arrowhead) is diffuse compared to that in pavement cells, and dark-staining fibrils (white arrows) reach from there into the cuticle. White arrowhead points to the epicuticular layer. Scale bar in (a-c) = 100 nm. (d) Thickness of different cuticle types, as indicated by the black bars in (a) and (c). Values given as means + *SD*, $n = 45$ (three measurements in three different images per cuticle type of five biological replicates). Statistical analysis used two-tailed unpaired Student's *t*-test, with $^{***}p < .001$. (e-f) Fluorol yellow staining of leaf cross-sections confirms a thicker cuticle over bulliform cells than over the neighboring pavement cells. FY = Fluorol Yellow (lipid stain), CW = Calcofluor White (cell wall counter stain). Scale bar in (e) = 50 nm, in (f) = 10 nm

BCs, on both sides of the leaf blade (Figure 4d) (Kessler et al., 2002). Cuticles of the excess bulliform-like cells in all three mutants exhibited Fluorol Yellow (FY) staining characteristics of normal BC cuticles (Figure 4f-i). FY staining of cuticles was used to quantify bulliform-like cells in the epidermis of all three mutants (Figure 4e). TEM was conducted to further investigate the cuticles of excess, bulliform-like cells in *wty2* and *Xcl1* mutants (Figure 5). The *dek1-D* mutant, whose comparably low coverage of abnormal epidermal cells did not allow for a clear identification of these cells in the high magnification but low-throughput setting of TEM, was omitted from this analysis. Cuticles of aberrant epidermal cells in both *wty2* (Figure 5b) and *Xcl1* (Figure 5c) mutants more closely resembled the cuticles of BCs in wild-type leaves (Figure 5a) than pavement cells (Figure 3a): increased cuticle thickness compared to a pavement cell cuticle, a diffuse cell wall/cuticle interface, and the lack of dark-light zonation within the cuticle proper as seen in pavement cell cuticles.

Since all three epidermal mutants displayed an increased number of bulliform-like cells on their surface, we further utilized them to investigate BC cuticle permeability during leaf dehydration (Figure 6). This was assessed by measuring epidermal water loss, also called cuticular conductance (g_c), of detached leaves in the dark to minimize stomatal water loss (Ristic et al., 2002; Lin et al., 2020). Mature adult leaves of all three bulliform-enriched mutants showed a significantly increased g_c compared to their wild-type siblings (Figure 6a). Although we cannot be certain that the bulliform-like cells in the three BC-enriched mutants have permeability characteristics identical to

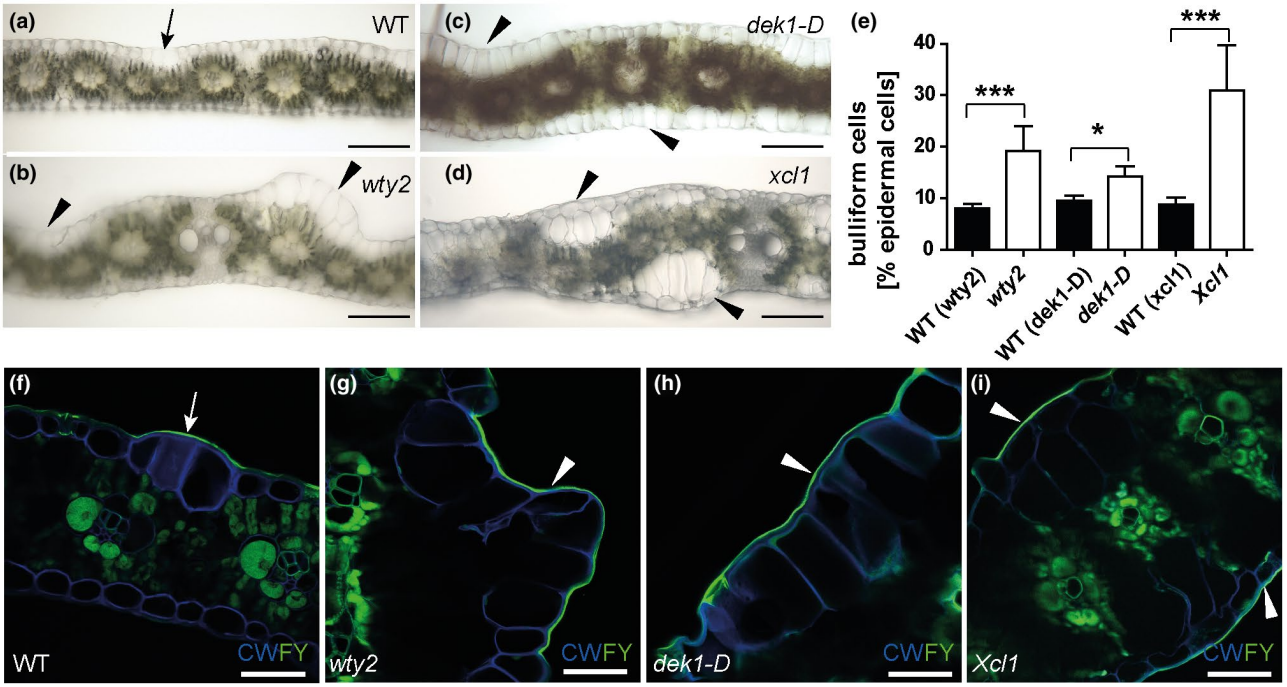

FIGURE 4 Three different epidermal mutants have increased bulliform cell coverage. (a-d) Bright field images of hand-sectioned adult leaves from the indicated genotypes depict previously reported aberrations in epidermal cell types. Arrow = wild-type-like bulliform strip (2 cells wide), arrowhead = areas with abnormal bulliform-like cells. Scale bar = 200 μm. (e) Quantification of bulliform cell number in three bulliform mutants as percentage of all epidermal cells, calculated using (f-i) Fluorol Yellow stained tissue cross section images. FY = Fluorol Yellow (lipid stain; green), CW = Calcofluor White (cell wall counter stain; blue). White arrow = FY staining of wild-type-like bulliform strip cuticle (3 cells wide), white arrowhead in (g-i) = areas with abnormal BC-like cells displaying increased FY staining of the cuticle. Scale bar = 50 μm. Values in (e) are given as means + *SD* (n = 300–380 epidermal cells counted, four biological replicates per genotype). Statistical analysis used two-tailed unpaired Student's *t*-test, with $^{*}p < .05$, $^{***}p < .001$

normal BCs, it is striking that all bulliform-enriched epidermises examined showed increased g_c, suggesting that the bulliform cuticle is more water permeable. To further investigate this possibility, we carried out a similar dehydration experiment comparing g_c of adaxial leaf surfaces of adult wild-type leaves (containing bulliform cells), to that of bulliform-free abaxial surfaces. This was achieved by covering one or the other surface with petroleum jelly to prevent water loss from the covered side of the leaf (Figure 6b). Consistent with elevated water permeability for bulliform cuticles, increased dehydration rates were observed for the bulliform-containing, adaxial side of the leaf compared to the abaxial, bulliform cell-free side, while the control without petroleum jelly constituted the full g_c. We note that epidermal hairs that could also elevate g_c are also present only on the adaxial side of the wild-type leaf, and investigated a possible role for hairs in raising g_c scores in bulliform-enriched mutants in the next section. Finally, as a third approach to explore the impact of BCs on g_c, we examined the relationship between BC coverage (Qiao et al., 2019) and g_c (Lin et al., 2020) in diverse inbred lines of the WiDiv panel (Lin et al., 2020). This analysis showed no correlation between BC strip coverage (number of BC strips x width) and g_c in the entire set of 447 lines with data for both traits (Figure S2a, Table S2), or in outliers with high and low BC coverage (Figure S2b), or high and low g_c scores (Figure S2c). The 2–3 fold variation in BC coverage in these lines may be too small, in relation to other factors impacting whole-leaf g_c in this diverse collection of inbred lines, to observe a relationship between BC coverage and g_c. In summary, our observations on g_c support the hypothesis that BC cuticles are more permeable to water in spite of their greater thickness.

3.5 | Bulliform cuticle nanoridges and adaxial hairs are not the main drivers of increased g_c in bulliform-enriched mutants

BCs show a reticulate pattern of cuticle nanoridges on their surfaces (Becraft et al., 2002), increasing cuticular surface area relative to overall cell surface area, and providing a possible explanation for increased g_c in bulliform-enriched mutants. To investigate this possibility, high resolution surface imaging of leaf glue impressions was performed with a Keyence VHX-6000 digital microscope system (Figure 7). BCs in wild-type leaves were organized in strips of 3–5 cells, and their cuticles displayed nanoridges aligned with the proximodistal axis of the leaf, often appearing to span cell-to-cell boundaries (Figure 7a-c). Adjacent pavement cells lacked these nanoridges. *wty2* mutants displayed normal bulliform strips as well as abnormal, epidermal "warts" which, upon closer inspection, revealed an even denser than normal pattern of cuticular nanoridges (Figure 7d-f). *dek1-D* mutants usually had wider than normal bulliform strips,

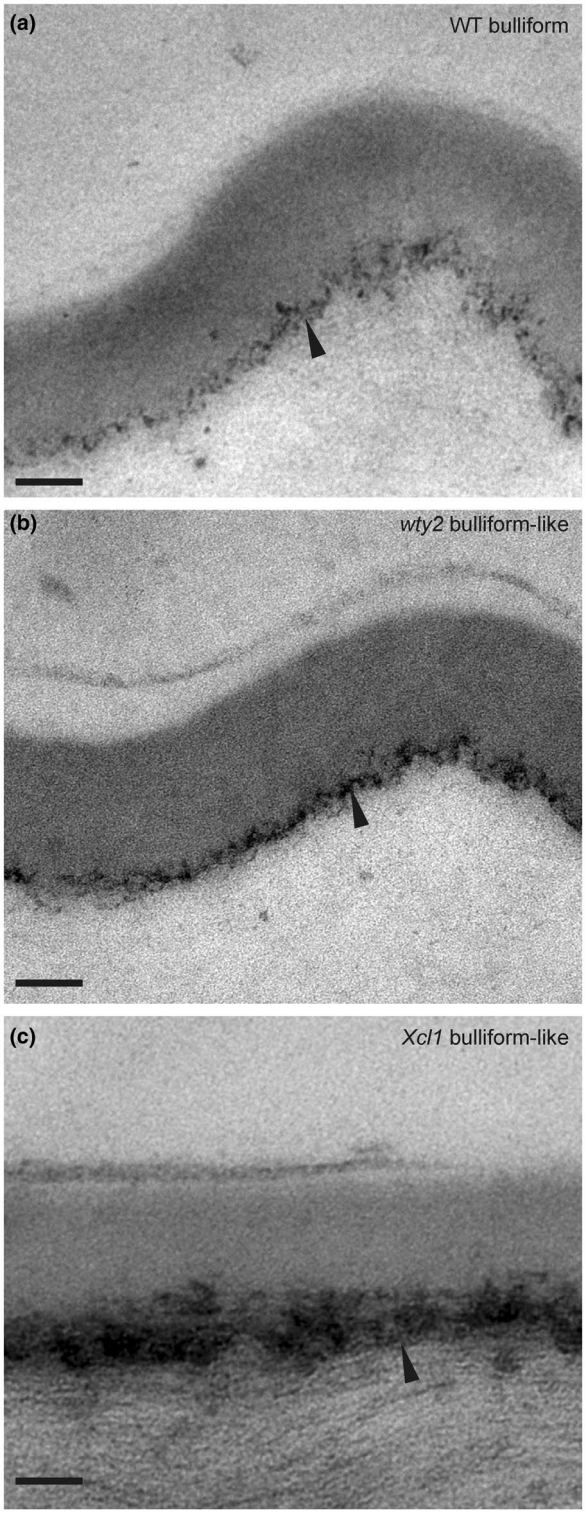

FIGURE 5 Cuticles of aberrant epidermal cells in bulliform-enriched mutants display BC-like ultrastructure. (a-c) Bulliform cell cuticle of wild-type (WT), *wty2*, and *Xcl1* mutant, visualized by TEM. Images in (b and c) display the outer surface of abnormal bulliform-like cells in the respective mutants, identified by the presence of related abnormal epidermal features of the area (warts in *wty2*, extra cell layer in *Xcl1*) before acquiring the TEM images. The black arrowhead indicates the diffuse cell wall/cuticle interface of bulliform cells (a) and bulliform-like cells (b, c). For comparison, images are shown in the same magnification as TEM images in Figure 3a and c. Scale bar = 100 nm

but cells in these strips varied with respect to cuticular nanoridges: cells in the center had nanoridges, whereas those towards the outer edges had few or no nanoridges (Figure 7g-i). Interestingly, in the last BC-enriched mutant, *Xcl1*, abnormal bulliform-like cells displayed no cuticular nanoridges (Figure 7j-l). These differences are not due to variations in leaf water content, as all leaves were fully turgid at the time glue impressions were made. Imaging of abaxial leaf impressions of some of the mutants (Figure S3) revealed bulliform-like cells on these usually bulliform-free surfaces. Bulliform-like cells with nanoridges could be observed in only some areas of the abaxial surface of *dek1-D*, while other areas had bulliform-like cells with smooth surfaces (Figure S3a,b). As seen for the adaxial surface, no nanoridges could be detected on the abaxial sides of *Xcl1* mutant leaves (Figure S3c,d). In conclusion, increased g_c observed in bulliform-enriched mutants cannot be caused solely by surface area increase due to the presence of cuticle nanoridges on their excess bulliform-like cells, since not all of the mutants displayed these cuticle features despite a higher cuticular conductance rate.

The presence of hairs on adaxial surfaces of wild-type leaves might contribute to their elevated g_c values, raising the question of whether increased hair density in BC-enriched mutants might at least partly account for the increased g_c observed in these mutants. To investigate this possibility, we quantified three different hair types: macrohairs, prickle hairs, and bicellular microhairs, on the adaxial surfaces of the three BC-enriched mutants. All three hair types (Figure S4a-h) were either significantly reduced in the mutant lines (Figure S4i-k), or did not show any difference in mutant compared to the wild-type. This excludes the possibility that the increased g_c rates detected in these mutants are due to increased hair density on the adaxial surface, and suggests that adaxial leaf hairs are not the main driver of higher g_c observed for adaxial wild type leaf surfaces relative to abaxial.

3.6 | Bulliform-enriched cuticles have a unique biochemical composition with major differences in cutin

In an effort to identify unique and functionally significant components of BC cuticles, we sought to biochemically characterize them. Since no method was available to physically separate bulliform from pavement cells on the scale needed to biochemically analyze their cuticles directly, two complementary approaches were again taken to compare these cuticle types indirectly with respect to both wax and cutin monomer composition: (a) adaxial (bulliform-containing) and abaxial (bulliform-free) cuticles were compared (see methods for information on how this was achieved), and (b) leaf cuticles of the bulliform-overproducing mutants (*wty2*, *dek1-D*, and *Xcl1*) were compared to their respective wild-type siblings. While there are other cellular differences in addition to BC content between adaxial and abaxial epidermises, and the cuticles of excess bulliform-like cells of

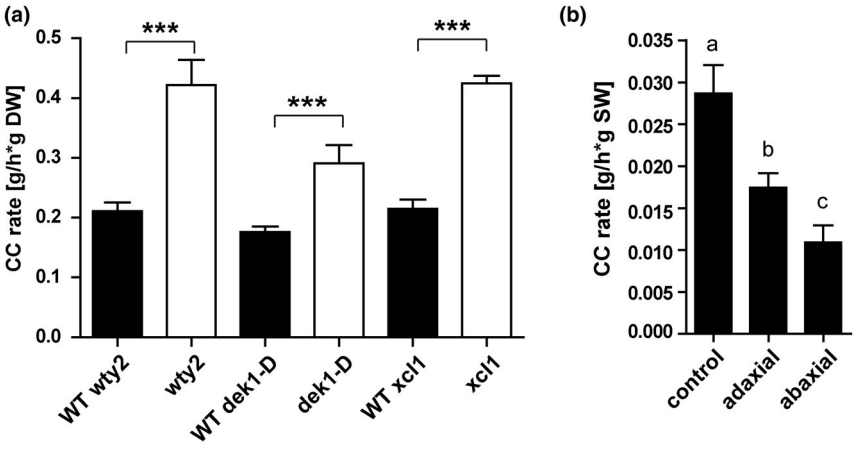

FIGURE 6 Bulliform-enriched tissues have increased cuticular conductance rates. Cuticular conductance, representing rates of water loss across the cuticle in the dark when stomata are closed, was measured during dehydration of detached leaves (20–22°C, 55%–65% humidity). (a) Cuticular conductance for three BC-enriched mutants *wty2*, *dek1-D*, and *Xcl1* and corresponding wild-types). CC rate is calculated as water loss (g) per hour per g dry weight (DW). Values are given as means + *SD* ($n = 3–5$ biological replicates per genotype). Statistical analysis used two-tailed unpaired Student's *t*-test, with $^{***}p < .001$. (b) Cuticular conductance rate of adaxial and abaxial leaf surfaces (one-sided dehydration was achieved by covering one side of the leaf with petroleum jelly) compared to full CC rate, calculated as water loss (g) per hour per g starting weight (SW). Values are given as means + *SD* ($n = 5–6$ biological replicates per surface). Statistical analysis used 1-way ANOVA, means with the same letter are not significantly different from each other; Tukey's post-test, $p < .05$

mutants may not be identical to those of normal bulliform cells, we reasoned that compositional differences seen in all comparisons are likely to provide insight into the composition of the BC cuticle.

The total lipid polyester (cutin) monomer load of wild-type adaxial cuticles was significantly higher than on the abaxial side (Figure 8a). The relative abundance of individual monomer classes in both adaxial and abaxial cuticles was determined via normalization to the total monomer load on the respective side. Some monomers, including 18:0 FA, several hydroxy FA, and DCAs, were reduced on the adaxial leaf surface (Figure 8a), while one compound, 18:0 9-epoxy-18-OH, showed a major accumulation in the adaxial surface containing BCs. All three bulliform-enriched mutant cuticles (Figure 8b) also had a higher total cutin monomer load compared to wild-type, thus we compared their relative lipid polyester monomer composition. Most monomers found to be different in the adaxial/abaxial comparison did not overlap or overlapped only partially with the differential abundances detected in the bulliform mutant analysis. However, the polar cutin component that is highly enriched in the BC-containing adaxial wild-type cuticles, 18:0 9-epoxy-18-OH, was also significantly increased in all three bulliform-enriched mutant cuticles. These findings point to 18:0 9-epoxy-18-OH as a cutin monomer that is likely enriched in BC cuticles.

Cuticular wax analysis of bulliform-enriched tissues created a more complex picture (Figure 9). Total wax load on the adaxial (bulliform-containing) side of wild-type leaves was increased (Figure 9a), but decreased in two of three of the bulliform-enriched mutants (Figure 9c). Relative amounts of individual wax types are presented in Figure 9b and d following normalization to the total wax load. A significant increase in hydrocarbons (alkanes and alkenes) was detected on the BC-containing adaxial side of wild-type leaves (Figure 9b), and hydrocarbons were also enriched in two of the three bulliform-enriched mutants (Figure 9d). The mutant where hydrocarbon enrichment was not observed (*dek1-D*) shows the weakest bulliform enrichment phenotype (Figure 4i), and could have failed to show the hydrocarbon enrichment seen in the other two mutants for this reason. Thus, most of the data support the possibility of hydrocarbon enrichment in BC cuticular waxes. No other wax classes showed relative abundance changes that were in agreement between adaxial/abaxial comparisons and bulliform mutants versus wild-type comparisons. While all three mutants showed increased free fatty acid content (Figure 9d), this difference was not seen in the adaxial/abaxial comparison (Figure 9b). Fatty alcohols and wax esters were decreased in two of the three mutants, but this difference was also not observed in the adaxial/abaxial analysis. Aldehydes, which were found to be decreased in adaxial (bulliform-containing) surface waxes, did not show a difference in the bulliform mutant comparisons. Analysis of single compounds within each wax class (Figure S5) also did not clearly point to specific wax molecules as specific to or enriched in BC cuticles. Thus, apart from evidence for hydrocarbon enrichment, we found no clear indication from these analyses of enrichment or depletion in individual wax classes or molecules in bulliform-enriched cuticles.

3.7 | Transcriptome analysis suggests a role of ferulate in BC cuticle maturation

In order to identify genes whose functions underlie unique features of BC cuticles, gene expression analysis of the three bulliform mutants was conducted. Here again, we employed the logic that while there are undoubtedly many differences in each individual mutants versus wild type comparison that are not relevant to BC ontogeny,

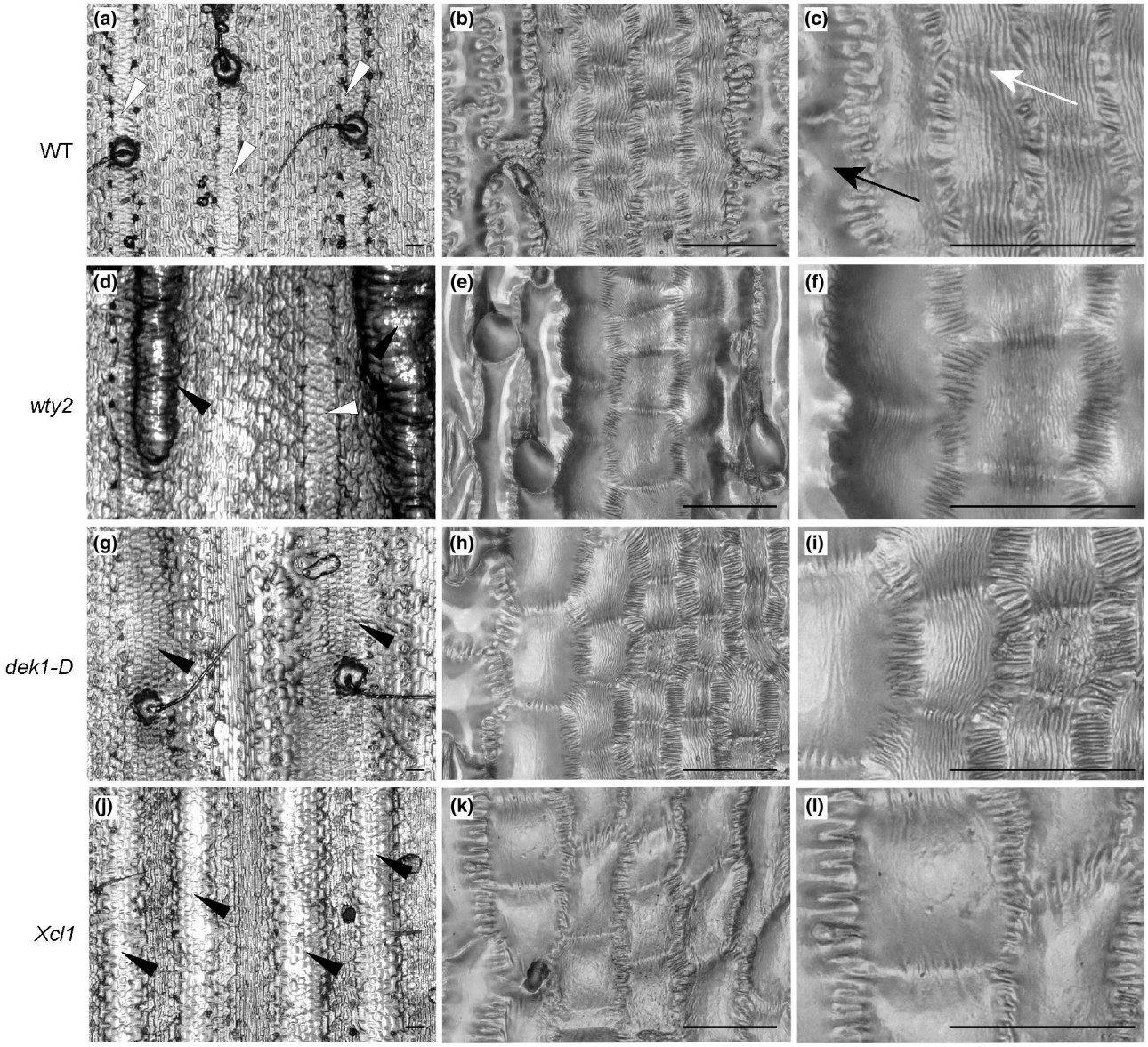

FIGURE 7 Bulliform-like cells in bulliform enriched mutants do not necessarily have cuticle nanoridges. Epidermal glue impressions of wild-type (a–c) and three bulliform-enriched mutants *wty2* (d-f), *dek1-D* (g-i), and *Xcl1* (j-l) at different magnifications. White arrowheads in (a and d) point to wild-type-like bulliform strips, while black arrowheads in (d, g, and j) mark abnormal bulliform strips. White arrow depicts nanoridges spanning cell-to-cell boundaries, black arrow indicates a pavement cell without cuticle nanoridges. In the middle and right columns, higher magnification views of bulliform-like cells in each genotype show their surface features in more detail. Note the absence of nanoridges on bulliform-like cells in *Xcl1* mutants. Scale bar in (a,d,g,j) = 100 μm, in all others 50 μm

genes differentially regulated in the same direction during cuticle maturation in all three mutants compared to wild-type can be considered candidates for genes involved in cuticle biogenesis. To this end, the previously characterized zone of cuticle maturation in developing adult leaves (from 10%–30% of the length of a partially expanded leaf #8; Bourgault et al., 2020) was harvested from mutants and corresponding wild-types, and analyzed via RNAseq (Figure 10, Figure S6). The three mutants displayed a varying degree of differential gene regulation, with 4,833 differentially expressed genes (DEG) for *wty2* in the analyzed zone (Figure S6a, Table S3), comparably less differential gene expression for *dek1-D* with only 132 DEG (Figure S6b, Table S4), and 527 DEG detected for *Xcl1* (Figure S6c, Table S5). However, the overlap between the DEGs in all three mutants was minimal, with only four genes showing a differential regulation in all three datasets (Figure 10a, Table S6), and only two of these genes deviating from wild-type values in the same direction in all three mutants (Figure 10b). One of these genes, *Zm00001d008957*, which showed increased expression in all three BC mutants, encodes a putative indole-3-acetic acid-amido synthetase and is annotated as *aas10* (auxin amido synthetase10). BLAST analysis identified AtJAR1, an enzyme responsible for the last step of the biosynthesis of bioactive jasmonic acid (JA), JA-Isoleucine, as its closest relative in

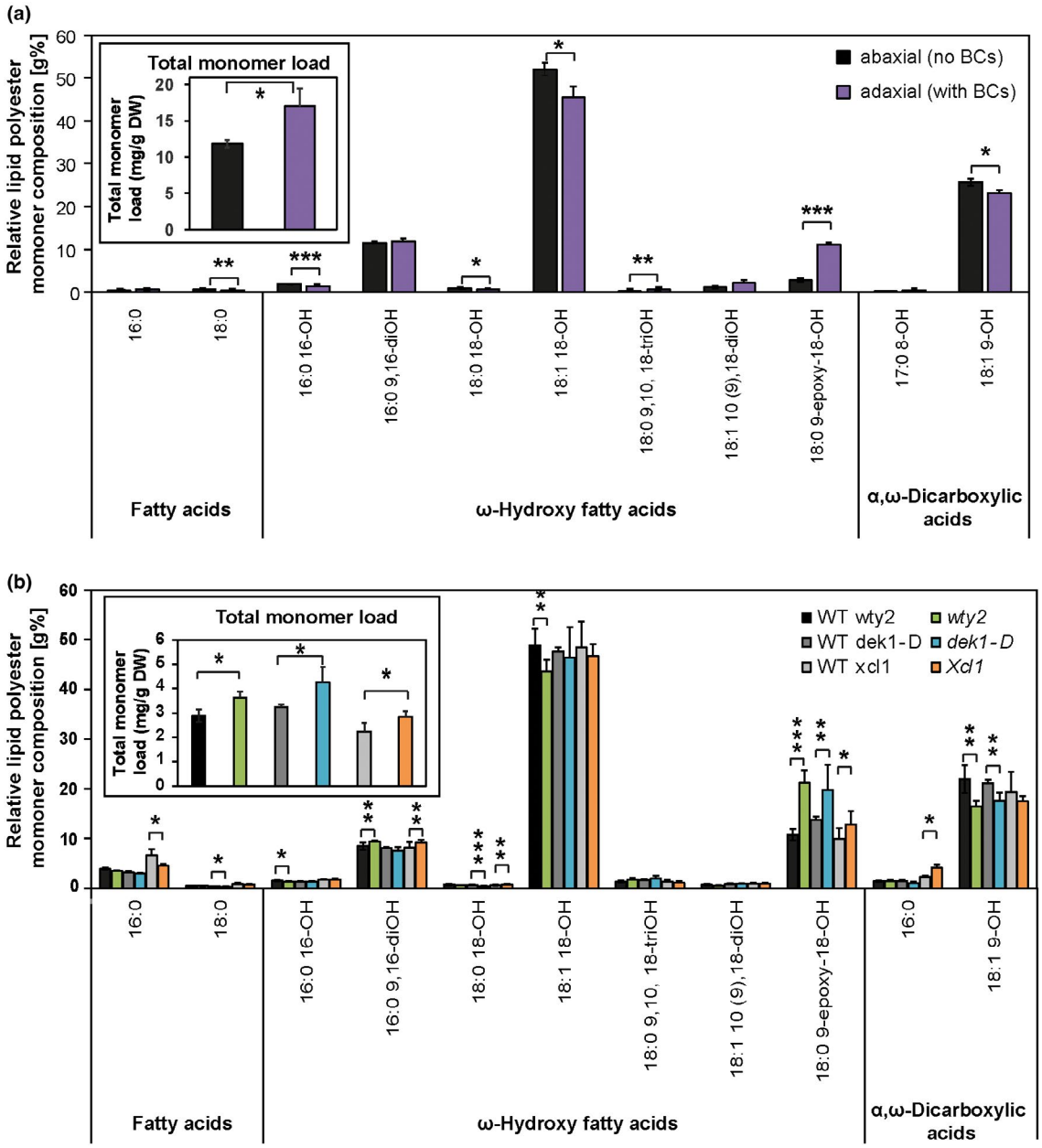

FIGURE 8 Bulliform-enriched cuticles have a unique biochemical composition with major differences in cutin. (a) Representative profile of cutin monomer composition of abaxial (BC-free) and adaxial (BC-containing) adult maize leaf surfaces, extracted and depolymerized from epidermal peels after enzymatic digestion, and measured via GC-MS. Monomer content of single compounds was normalized to overall cutin monomer load (inset). (b) Representative profile of cutin monomer composition of bulliform-enriched mutants after whole-tissue extraction and depolymerization, measured via GC-MS. Monomer content of single compounds was normalized to overall cutin monomer load (inset). Values are given as means ± *SD* ($n = 4$ biological replicates per surface/genotype). Statistical analysis used two-tailed unpaired Student's *t*-test, with $^{*}p < .05$, $^{**}p < .01$, and $^{***}p < .001$. The cutin chromatographic traces contained 11 unidentified peaks, where the total unidentified peak area corresponded to 2.7 ± 0.2% (adaxial cutin) and 3.2 ± 0.05% (abaxial cutin) of the total integrated area (unidentified + identified)

Arabidopsis (Table S7). Other Arabidopsis proteins with high amino-acid sequence identity to AAS10 mostly belong to the auxin-responsive GH3 protein family.

The other gene differentially regulated in the same direction in all three BC mutants (reduced expression) is *Zm00001d050455*, which is not functionally annotated in the maize genome but its closest relative in Arabidopsis encodes a hydroxy-cinnamoyl-CoA shikimate/quinate hydroxy-cinnamoyl transferase in Arabidopsis (HCT described by Hoffmann et al., 2004; 37% identical at the protein level) (Table S8). Interestingly, a slightly less similar gene (28% identity at the protein level, Table S8) encodes *DEFICIENT IN CUTIN FERULATE* (*DCF*) in Arabidopsis. Defects in this gene lead to an almost complete absence of the HCA compound ferulate in the cutin fraction of rosette leaf cuticles (Rautengarten et al., 2012).

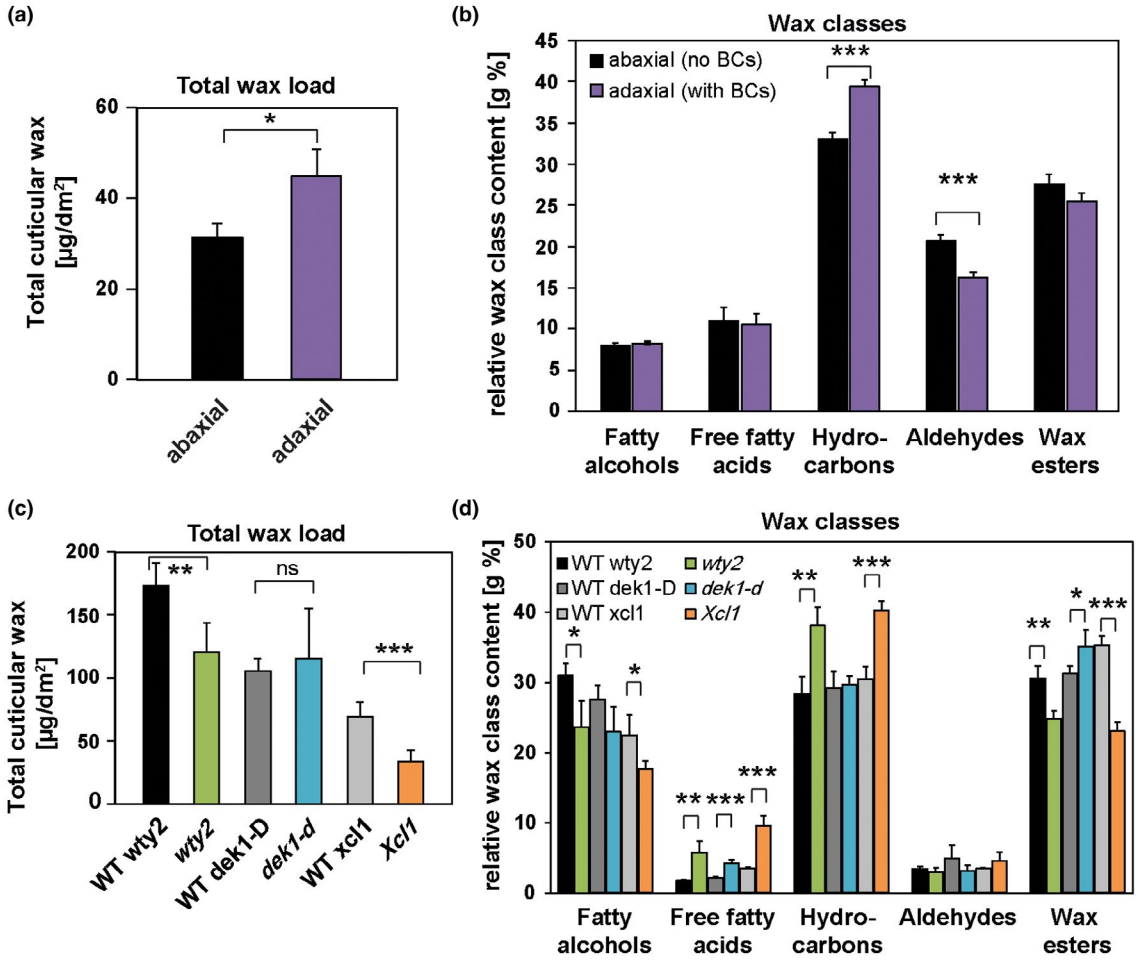

FIGURE 9 Wax profiles of bulliform-enriched cuticles are diverse. (a) Total wax load of abaxial (BC-free) and adaxial (BC-containing) leaf surfaces, chloroform-extracted from one leaf surface or the other, and measured by GC-MS. (b) Relative content of wax classes in adaxial and abaxial tissues after normalization to overall wax load. (c) Total wax load of bulliform-enriched mutants after chloroform extraction of both leaf surfaces. (d) Content of wax classes in bulliform-enriched mutants was normalized to overall wax load. Values are given as means ± *SD* ($n = 4$ biological replicates per surface/genotype). Statistical analysis used two-tailed unpaired Student's *t*-test, with $^{*}p < .05$, $^{**}p < .01$, and $^{***}p < .001$

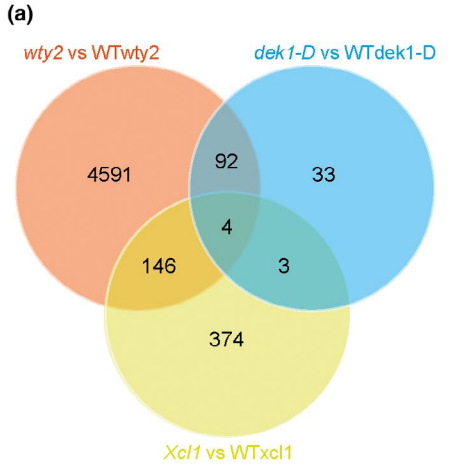

Zm00001d008957	Indole-3-acetic acid-amido synthetase GH3.6; aas10 - auxin amido synthetase10
Zm00001d035561	Expressed protein; Mannose-specific jacalin-related lectin; (reversible sugar binding)
Zm00001d046210	Beta-glucosidase 11 (hydrolysis of beta-d-glucosidic bonds)
Zm00001d050455	Anthranilate N-benzoyltransferase protein 1; hydroxycinnamoyl-CoA shikimate/quinate hydroxycinnamoyl transferase

FIGURE 10 Transcriptomic analysis of the cuticle maturation zone in bulliform-enriched mutants. (a) Venn diagram depicts overlap of differentially expressed genes (DEGs) for all three bulliform mutants. (b) Gene identifiers and putative gene function of four DEGs identified in all three bulliform mutant comparisons. *w* = *wty2*, *d* = *dek1-D*, and *X* = *Xcl1*, red arrow = gene expression is increased. green arrow = gene expression is decreased in the respective mutant

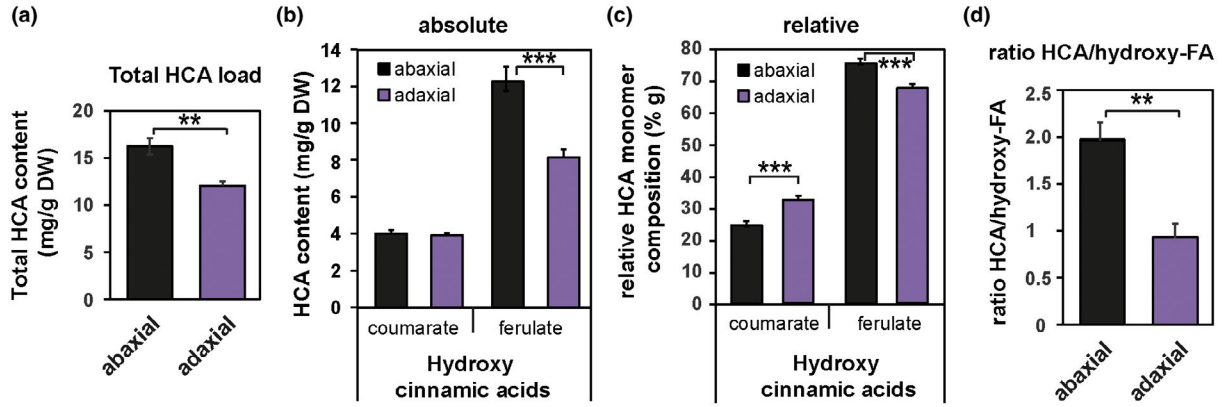

FIGURE 11 Ferulate is depleted in the adaxial (bulliform-containing) cuticle. (a) Total hydroxycinnamic acid (HCA) content of abaxial and adaxial leaf surfaces, extracted and depolymerized from epidermal peels after enzymatic digestion, and measured by GC-MS. (b) Absolute and (c) Relative content of coumarate and ferulate in abaxial versus adaxial tissues. (d) Ratio of total HCA content to total hydroxy fatty acid (FA) content in abaxial and adaxial tissue. Values are given as means ± *SD* ($n = 4$ biological replicates per surface). Statistical analysis used two-tailed unpaired Student's *t*-test, with $^{**}p < .01$ and $^{***}p < .001$

Both enzymes belong to the HXXXD/BAHD acyltransferase family, where some members are characterized to catalyze acyl transfer reactions between CoA-activated hydroxycinnamic acid derivatives and hydroxylated aliphatics in the formation of lipid barriers like suberin or cutin (Molina & Kosma, 2015). A phylogenetic analysis of selected BAHD family acyltransferases from maize and other organisms (Figure S7, after Molina & Kosma, 2015) positioned the maize candidate Zm00001d050455 (light blue) with several other designated maize "HCT" proteins in a distinct subclade within the HCT clade (dark blue), which might have evolved different functions than HCT. This led us to investigate whether the reduced expression of *Zm00001d050455* in bulliform-enriched tissue indeed has an influence on HCA content specifically in the BC-enriched cuticle by using our previously described dataset. In the comparison of wild-type adaxial versus abaxial cutin, isolated from epidermal peels, decrease in HCAs could be observed on the adaxial (bulliform-containing) side (Figure 11a), which was solely due to reduced ferulate content (Figure 11b). Analysis of relative HCA content revealed an increase in coumarate and decrease in ferulate in the adaxial cuticle (Figure 11c). Comparing the ratio of HCAs to their potential acceptor molecules hydroxy-FAs between adaxial and abaxial cutin monomers (Figure 11d), we observed a significantly reduced HCA/hydroxy-FA ratio in adaxial tissue. Together, these findings suggest that BC cuticles are indeed reduced in ferulate, supporting the hypothesis that the putative HCA biosynthetic gene product of *Zm00001d050455* likely supplies ferulate for incorporation into the cutin polyester and is downregulated in BCs relative to other epidermal cells (Figure 10,) leading to reduced ferulate content of BC-rich cuticles. This analysis could not be readily extended to BC-enriched mutants because cutin analysis conducted on these mutants utilized whole leaves (not epidermal peels), thereby including internal tissue. Previous work showed that that most HCAs in samples prepared this way are of non-epidermal origin (Bourgault et al., 2020) so they are not informative regarding cuticular HCA content. In summary, analysis of gene expression in BC-enriched mutants suggests roles for hormone and HCA biosynthesis in BC differentiation. These results combined with analysis of HCA content in adaxial versus abaxial cuticles suggest that ferulate biosynthesis is downregulated during cuticle maturation to achieve reduced ferulate content in BC-enriched cuticles relative to other epidermal cell types.

4 | DISCUSSION

Variability in cuticle composition and structure is found between different plant species, developmental stages and tissue types (Jeffree, 2006; Jetter et al., 2006). The functions of distinct cell types within a single tissue might require different surface properties, and consequently cuticle types, to support these functions. This study set out to investigate BC cuticles in maize, the function of BCs in leaf rolling upon dehydration, and how cuticle properties may be related to the function of this unique epidermal cell type.

4.1 | Maize leaf rolling is impacted by bulliform strip patterning

The role of BCs in leaf rolling has been a matter of ongoing debate for decades, and no clear conclusion has been drawn about their functional contribution to this important drought response (Ellis, 1976; Moulia, 2000). Loss of turgor in BCs located only on the adaxial leaf surface has long been thought to induce rolling with additional contribution by shrinkage of subepidermal sclerenchyma and mesophyll tissue due to water loss (Redmann, 1985). Our study provides direct evidence of this proposed role for BCs by demonstrating differential shrinkage of bulliform cells upon dehydration of maize leaves using a novel cryo-confocal imaging technique. However, rolling can also occur in leaves that lack BCs (Shields, 1951), questioning the necessity of this cell type for the leaf rolling response. The present study further investigated

a functional role for BCs in leaf rolling in maize by examining the relationship between bulliform patterning and leaf rolling across a large collection of genetically diverse maize lines. Data on bulliform strip pattern collected for a GWAS of this trait (Qiao et al., 2019) were analyzed in relation to rolling rate data of excised leaves collected for the same plants. Faster rolling speed was positively correlated with bulliform strip frequency and negatively correlated with bulliform strip width, indicating that rolling is facilitated by more closely spaced and narrower bulliform strips. To our knowledge, no other study has analyzed the impact of BC architectural variation in grasses on leaf rolling. A study on the flag leaf in wheat revealed that a drought-resistant variety, exhibiting faster leaf rolling than a comparable drought-susceptible genotype, had larger BCs, possibly contributing to the faster rolling response, but also other altered features like differences in cuticular composition (Willick et al., 2018). No information about the BC architecture across the leaf was collected in this case.

Our findings add to prior observations that many leaf rolling mutants in rice or maize show alterations in BC size, number or adaxial/abaxial positioning (Gao et al., 2019; Nelson et al., 2002; Xu et al., 2018). Leaf architecture in general seems to be important, as histological analyses of a collection of 46 adaxially or abaxially rolled mutants in rice showed that changes of number, size, and pattern of BCs, sclerenchyma cells, parenchyma cells, and mesophyll cells as well as vascular bundles all could cause altered leaf rolling (Zou et al., 2014). However, these mutations usually lead to a constantly rolled leaf status rather than alterations in the inducibility or speed of rolling upon drought or heat stress. Our leaf rolling analysis was done on excised leaves, which might not perfectly mirror leaf rolling behavior in a drought- or heat-stressed intact plant. Nevertheless, our data support the conclusion that bulliform strip architecture and distribution across the leaf play a role in regulation of stress-induced leaf rolling. Although a microscopic phenotype, bulliform strip patterning could represent an important agronomic trait with consequences on macroscopic phenotypes such as plant architecture and drought resistance.

4.2 | BC cuticles of the adult maize leaf are structurally and compositionally unique

In the adult maize leaf, pavement cells, BCs, and stomatal guard and subsidiary cells all show distinct cuticle ultrastructure (Bourgault et al., 2020). The present study examined the ultrastructure of BC cuticles in detail. Compared to pavement cells, cuticles of BCs are roughly fourfold thicker and are further distinguished by having a prominent cuticular layer defined by the presence of osmiophilic fibrils oriented perpendicular to the plane of the cuticle, likely to be polysaccharides (Jeffree, 2006; Mazurek et al., 2017). The presence of a cuticular layer likens the BC cuticle more to the classic three-layered cuticle model than the pavement cell cuticle of maize leaves, which lack a well-defined cuticular layer but have two distinct layers of the cuticle proper (Bourgault et al., 2020).

This study investigated the composition of the BC cuticle via correlative strategies taking advantage of differences in BC density between leaf tissues of different genotypes or anatomical locations. In wild-type adult maize leaves, BCs are present only on the adaxial surface, but the thickness and ultrastructure of pavement cell cuticles are indistinguishable on adaxial and abaxial surfaces (Bourgault et al., 2020). Thus, differences we observed in cuticle composition between the two surfaces are likely due primarily to the presence of BCs and other cell types (e.g. hairs) present only on the adaxial side. A complementary analysis of bulliform-enriched tissue was undertaken by comparing three different bulliform-enriched mutants (*wty2*, *dek1-D*, and *Xcl1*) to their respective wild-type siblings. Since BC-enriched mutants have either unchanged or significantly decreased adaxial hair density, it is likely that the compositional differences observed in all comparisons (bulliform mutants versus. wild-type, and adaxial versus. abaxial wild-type) reflect a true compositional difference between BC and pavement cell cuticles, potentially identifying important functional components of this specialized cuticle type.

An overall increase in cutin (but not wax) load was found in bulliform-containing or -enriched tissue in all the comparisons. This increase is consistent with the dramatically increased thickness of the BC cuticle, an increase that is mostly due to the presence of a (presumed cutin-containing) cuticular layer not present in pavement cell cuticles. Moreover, all comparisons agreed in identifying an enrichment in bulliform cuticles of the cutin monomer 9,10-epoxy-18-hydroxyoctadecanoic acid. Together, our findings identify cutin load and monomer composition as the main differences between BC-enriched and their respective control cuticles, potentially changing the physical properties of the cuticle, maybe due to altered cross-linking (Fich et al., 2016) or to higher polarity of the monomer constituents in the polymer scaffold. Analysis of the petal cuticle in Arabidopsis revealed that cutin biosynthesis is required for the formation of cuticle nanoridges (Li-Beisson et al., 2009; Mazurek et al., 2017), supporting the idea that nanoridges found on the BC cuticle might be present due to different cutin load and/or composition, likely resulting a different polyester structure compared to pavement cells, which lack nanoridges. The functional significance of 9,10-epoxy-18-hydroxyoctadecanoic acid in the BC cuticle is unclear, but it has previously been implicated in freeze-resistance of cold-hardened rye (Griffith et al., 1985). Interestingly, this monomer was found to be the dominating cutin component in the mature leaf portion of *Clivia miniata*, where its accumulation is thought to indicate that the possible maximum of cross-linking in the cutin fraction had not been achieved (Riederer & Schönherr, 1988). High content of monomers with unused functional groups for cross-linking, like epoxy substituents, can indicate a reduced proportion of actual cross-linking (Riederer & Schönherr, 1988) suggesting a looser cutin scaffold. The ability to draw definitive conclusions about differences in cuticle composition between BCs and other epidermal cell types is limited by the inability to isolate these cells in sufficiently large quantities for biochemical analysis of cuticles. A promising avenue for future analyses of cuticle specializations in BCs and other epidermal

cell types would be the employment of single-cell in-situ-imaging techniques, previously shown with e.g. Infrared (IR), FTIR (Fourier transform IR) (Mazurek et al., 2013), Raman scattering spectroscopy techniques (Weissflog et al., 2010; Yu et al., 2008), or compositional analysis of waxes or cutin via matrix-assisted laser desorption/ionization mass spectrometry imaging (MALDI-MSI) (Cha et al., 2009; Veličkovic et al., 2014). Jun et al. (2010) achieved a spatial resolution of ~12 μm in MS-imaging of flower tissue in Arabidopsis, with single pixel profiles demonstrating single-cell-level spatial resolution, allowing for semi-quantification of surface metabolites on single pixels of the flower tissue. Although these techniques require very specialized equipment and expertise, application of these and related methods seem to be able to deliver cell-to-cell resolution of cuticle composition.

Gene expression analysis of BC-enriched mutants yielded fewer candidate regulators of BC differentiation than anticipated, but identified two genes that were differentially expressed in the same direction in the cuticle maturation zone of all three mutants compared to wild-type. One of these, *Zm00001d050455*, is a homolog of *Arabidopsis HCT*, which is involved in phenylpropanoid biosynthesis (Hoffmann et al., 2004). Another member of this gene family in Arabidopsis, *AtDCF*, encodes a protein that promotes ferulate esterification into the growing cutin polymer (Rautengarten et al., 2012). Both enzymes are members of the BAHD family of acyltransferases, which includes enzymes that contribute to the formation of extracellular lipid barriers. While AtDCF exhibits feruloyl-CoA transferase activity in the epidermis, recognizing several different substrates in vitro (Rautengarten et al., 2012), another family member in Arabidopsis (AtFACT) was shown to act as a caffeoyl-CoA transferase in suberin biosynthesis (Kosma et al., 2012). Loss of function of other members with unknown enzymatic activity can result in compositional changes of either cutin or even cuticular waxes (Molina & Kosma, 2015). The reduced expression of *Zm00001d050455* observed in all three BC-enriched mutants could suggest a possible role for this gene in HCA deposition in cuticles. While a function similar to HCT would predict a role in ferulate biosynthesis, a function similar to DCF would suggest reduced incorporation of ferulate into the polyester upon downregulation of the gene in BCs. Phylogenetic analysis positioned the candidate closer to the HCT clade than to proteins related to extracellular lipid biosynthesis like DCF, but the localization in a distinct subclade with several other designated "HCT" maize proteins might suggest that these genes might not be true homologs of HCT either and could have other distinct functions that affect hydroxycinnamic acid accumulation, maybe even specifically in the cuticle. In any case, comparative analysis of abaxial versus adaxial cutin composition provided evidence that BC cuticles do indeed have reduced ferulate content compared to pavement cells, but a role for *Zm00001d050455* in establishing this difference remains to be confirmed. While HCAs have been described to show antioxidant as well as antimicrobial properties in general (Domergue & Kosma, 2017) the functional role of ferulate in the cuticle remains unclear. Analyses of cuticle permeability in Arabidopsis mutants lacking the *DCF* gene suggest that cutin-bound ferulate does not affect structural and sealing properties of the cuticle (Rautengarten et al., 2012). Just as single cell analysis would provide more definitive insights into cell type differences in cuticle composition, more precise and definitive information about gene expression differences underlying the unique structural and compositional features of BC cuticles could be achieved in future work using single-cell RNA-sequencing strategies after isolating BCs from the cuticle maturation zone by techniques such as laser-capture microdissection or microfluidics (Chen et al., 2019).

4.3 | Bulliform-enriched tissue shows increased water loss upon dehydration

We showed that wild-type adaxial leaf surfaces containing BCs displayed higher g_c than the abaxial surfaces lacking BCs. A contribution from the other main adaxial-only cell type, epidermal hairs, to increased g_c is possible, but we also observed increased g_c rates for leaves of three bulliform-enriched mutants, which all have either unchanged or reduced density of adaxial hairs. Together, these findings strongly suggest that BCs lose water across the cuticle at a faster rate than pavement cells. While studies of g_c have investigated this trait in a multitude of plant species (e.g. table 1 in Kerstiens, 1996), only a few compare the g_c of adaxial and abaxial tissues. For example, no difference in g_c between adaxial and abaxial leaf surfaces could be measured for holm oak (Fernández et al., 2014) or beech (Hoad et al., 1996). While these are dicot species lacking BCs on their adaxial surface, a study in rice also showed increased adaxial g_c in leaves (Agarie et al., 1998), in agreement with our results of higher water loss rates from bulliform-containing tissue.

Is it likely that the much thicker BC cuticle is more water permeable? While some data connect a thicker cuticle to a lower cuticular water loss rate in maize (Ristic et al., 2002), there is a long line of evidence that cuticle composition is the main determinant of water permeance rather than thickness (Buschhaus & Jetter, 2012; Jetter & Riederer, 2016; Kerstiens, 1996; Riederer & Schreiber, 2001). For example, several mutants with altered wax and cutin composition showed higher cuticle permeability despite increased cuticle thickness (Kurdyukov et al., 2006; Sadler et al., 2016; Xiao et al., 2004). The differential accumulation of epoxy-monomers in the cutin fraction of BC-enriched tissue might be an indication of a cutin scaffold with modified cross-linking, since cuticles high in these monomers with unused functional groups for cross-linking are assumed to show a lower degree of cross-linking (Riederer & Schönherr, 1988). Altered polymer structure in the BC cuticle due to modified cross-linking could impact the organization of associated waxes, with consequences for water permeability. Also, higher polarity of cutin monomer constituents in the polymer scaffold, like the epoxy-monomer in BC-enriched tissue, could facilitate water passage through the BC cuticle. In fact, it has been shown that increasing amounts of water can go through polar domains of the cuticle with increasing humidity and, as a consequence, cuticular permeability increases (Schreiber, 2005). Moreover, existence of a layer with polysaccharide fibrils in the BC

cuticle could indicate an aqueous connection for easier water passage through the matrix of cutin and waxes with hydrophilic domains provided by polysaccharides (Fernández et al., 2017). While a reduction in cutin ferulate in Arabidopsis did not change the barrier properties of the cuticle (Rautengarten et al., 2012), ectopic expression of a poplar hydroxyacid hydroxycinnamoyl-transferase in Arabidopsis led to an increase in ferulate in cutin and suberin (Cheng et al., 2013), functionally providing increased resistance to salt stress. The authors speculate that this is likely a result of increased impermeability of the lipid barrier due to the elevated ferulate content. Thus, the reduction of ferulate we observed in the BC-enriched cuticle surface, in combination with other compositional changes, might increase cuticle permeability leading to increased water loss across BC-enriched cuticles.

We could not identify a consistent relationship between the enrichment of BCs and the amount of waxes deposited in the cuticle. While the adaxial leaf surface had an increased wax load compared to abaxial tissue (which also could stem from other adaxial cell types like hairs), 2 of 3 BC-enriched mutants showed a significant reduction in wax content. Although we also did not detect consistent changes in wax composition in all BC-enriched tissues examined, hydrocarbons were elevated in most BC-enriched tissues. At first, this increase would be counterintuitive for a more permeable cuticle, since alkanes are usually associated with increased water barrier properties, e.g. in drought stress conditions (Leide et al., 2007; Kosma et al., 2009). However, increased deposition of these wax components might support the water barrier of BC cuticles, potentially necessary due to alterations in the cutin matrix. For example, increased wax load observed in cutin mutants has been postulated to compensate for the insufficient cutin scaffold (Bessire et al., 2007; Kurdyukov et al., 2006).

BCs show increased volume loss upon leaf dehydration compared to adjacent pavement cells, as shown by cryo-confocal analysis of dehydrated tissue. This differential shrinkage might involve cell-type specific ion exchange and resulting changes in osmotic potential and water movement from BCs to neighboring cells, similar to what occurs during stomatal closure. However, our evidence of elevated g_c for BC-enriched tissue compared to the respective controls raises the possibility that increased water permeability of the bulliform cuticle may contribute to the differential shrinkage of these cells during leaf dehydration. Indeed, during our leaf dehydration assays, water is not only being re-distributed among leaf cells but is lost by evaporation (as indicated by gradually decreasing weight of the detached leaf). Importantly, all our leaf dehydration experiments, including the cryo-confocal imaging experiment, were conducted in the dark to minimize stomatal transpiration, so water is being lost mainly via evaporation across the cuticle. Thus, a higher water loss rate across the bulliform cuticle may accelerate BC volume loss, and in this way, the specialized bulliform cuticle may contribute to bulliform function in leaf rolling.

5 | CONCLUDING REMARKS

In conclusion, we demonstrate that maize BCs shrink differentially upon dehydration and have a specialized cuticle architecture compared to pavement cells, and that BC-enriched tissues have altered cuticle composition and elevated g_c rates. The exact role of BCs and their specialized cuticle in the leaf rolling response of maize has yet to be elucidated, but we hypothesize that a thicker, yet more water permeable cuticle contributes to differential shrinkage of BCs upon leaf dehydration, and thus to leaf rolling. Integration of biochemical, transcriptomic, ultrastructural, and functional data suggest an important role for the cutin matrix in this cuticle type, including the compound 9,10-epoxy-18-hydroxyoctadecanoic acid. Together, our findings advance knowledge of cuticle composition/structure/function relationships, and how cuticle specialization can contribute to cell and organ functions.

ACKNOWLEDGMENTS

We thank Prof. Anne Sylvester (University of Wyoming), Prof. Phil Becraft (Iowa State University), and Prof. Neelima Sinha (UC Davis) for donation of seeds. We also thank Prof. Siobhan Braybrook (UC Los Angeles) for use and help with the Keyence imaging system equipment. This work was financially supported by U.S. National Science Foundation IOS1444507, a Deutsche Forschungsgemeinschaft (DFG) Fellowship (MA-7608/1-1) to SM, and by funding from the Canada Research Chairs program (CRC) to IM.

CONFLICT OF INTEREST

The authors declare that the research was conducted in the absence of any commercial or financial relationships that could be construed as a potential conflict of interest.

AUTHOR CONTRIBUTIONS

SM, IM, and LGS conceived the project and designed experiments. SM and MFV conducted most experiments. RB and IM performed GC-MS analysis of cuticle composition, and PS and SM performed cryo-microscopy. JC, NK, MAG, and LGS helped to establish and conduct the leaf rolling assay. SM, RB, IM, and LGS analyzed data. SM and LGS wrote the article with contributions of all authors.

ORCID

Susanne Matschi https://orcid.org/0000-0001-6233-2519
Richard Bourgault https://orcid.org/0000-0002-9502-8801
Michael A. Gore https://orcid.org/0000-0001-6896-8024
Isabel Molina https://orcid.org/0000-0003-3450-893X
Laurie G. Smith https://orcid.org/0000-0002-8294-1589

REFERENCES

Agarie, S., Uchida, H., Agata, W., Kubota, F., & Kaufman, P. B. (1998). Effects of silicon on transpiration and leaf conductance in rice plants (*Oryza sativa L.*). *Plant Production Science*, *1*, 89–95.

Altschul, S. F., Madden, T. L., Schäffer, A. A., Zhang, J., Zhang, Z., Miller, W., & Lipman, D. J. (1997). Gapped BLAST and PSI-BLAST: A new generation of protein database search programs. *Nucleic Acids Research*, *25*, 3389–3402. https://doi.org/10.1093/nar/25.17.3389

Anders, S., & Huber, W. (2010). Differential expression analysis for sequence count data. *Genome Biology*, *11*, R106.

Anders, S., Pyl, P. T., & Huber, W. (2015). HTSeq–a Python framework to work with high-throughput sequencing data. *Bioinformatics*, *31*, 166–169. https://doi.org/10.1093/bioinformatics/btu638

Bargel, H., Koch, K., Cerman, Z., & Neinhuis, C. (2006). Evans Review No. 3: Structure-function relationships of the plant cuticle and cuticular waxes - a smart material? *Functional Plant Biology*, *33*, 893–910.

Becraft, P., Li, K., Dey, N., & Asuncion-Crabb, Y. (2002). The maize *dek1* gene functions in embryonic pattern formation and cell fate specification. *Development*, *129*, 5217–5225.

Bessire, M., Chassot, C., Jacquat, A.-C., Humphry, M., Borel, S., Petétot, J.- M.-C., Métraux, J.-P., & Nawrath, C. (2007). A permeable cuticle in Arabidopsis leads to a strong resistance to *Botrytis cinerea*. *EMBO Journal*, *26*, 2158–2168. https://doi.org/10.1038/sj.emboj.7601658

Bianchi, A., & Marchesi, G. (1960). The surface of the leaf in normal and glossy maize seedlings. *Zeitschrift Fur Vererbungslehre*, *91*, 214–219. https://doi.org/10.1007/BF00890032

Bianchi, G., & Avato, P. (1984). Surface waxes from grain, leaves, and husks of maize (*Zea mays L.*). *Cereal Chemistry*, *61*, 45–47.

Bongard-Pierce, D. K., Evans, M. M. S., & Poethig, R. S. (1996). Heteroblastic features of leaf anatomy in maize and their genetic regulation. *International Journal of Plant Sciences*, *157*, 331–340. https://doi.org/10.1086/297353

Bourgault, R., Matschi, S., Vasquez, M., Qiao, P., Sonntag, A., Charlebois, C., Mohammadi, M., Scanlon, M. J., Smith, L. G., & Molina, I. (2020). Constructing functional cuticles: Analysis of relationships between cuticle lipid composition, ultrastructure and water barrier function in developing adult maize leaves. *Annals of Botany*, *125*, 79–91. https://doi.org/10.1093/aob/mcz143

Buschhaus, C., Herz, H., & Jetter, R. (2007). Chemical composition of the epicuticular and intracuticular wax layers on adaxial sides of *Rosa canina* leaves. *Annals of Botany*, *100*, 1557–1564. https://doi.org/10.1093/aob/mcm255

Buschhaus, C., & Jetter, R. (2012). Composition and physiological function of the wax layers coating Arabidopsis leaves: β-Amyrin negatively affects the intracuticular water barrier. *Plant Physiology*, *160*, 1120–1129. https://doi.org/10.1104/pp.112.198473

Cha, S., Song, Z., Nikolau, B. J., & Yeung, E. S. (2009). Direct profiling and imaging of epicuticular waxes on *Arabidopsis thaliana* by laser desorption/ionization mass spectrometry using silver colloid as a matrix. *Analytical Chemistry*, *81*, 2991–3000. https://doi.org/10.1021/ac802615r

Cheng Ai-Xia, Gou Jin-Ying, Yu Xiao-Hong, Yang Huijun, Fang Xin, Chen Xiao-Ya, & Liu Chang-Jun (2013). Characterization and ectopic expression of a *populus* hydroxyacid hydroxycinnamoyltransferase. *Molecular Plant*, *6*, (6), 1889–1903. http://dx.doi.org/10.1093/mp/sst085

Chen, G., Ning, B., & Shi, T. (2019). Single-Cell RNA-Seq technologies and related computational data analysis. *Front Genet*, *10*, 317. https://doi.org/10.3389/fgene.2019.00317

Domergue, F., & Kosma, D. K. (2017). Occurrence and biosynthesis of alkyl hydroxycinnamates in plant lipid barriers. *Plants (Basel, Switzerland)*, *6*, 25. https://doi.org/10.3390/plants6030025

Duval-Jouve, M. (1875). Histotaxie des feuilles de graminées. *Bull La Société Bot Fr*, *22*, 115–117. https://doi.org/10.1080/00378941.1875.10825591

Ellis, R. P. (1976). A procedure for standardizing comparative leaf anatomy in the Poaceae. II. The epidermis as seen in surface view. *Bothalia*, *12*, 65–109.

Espelie, K. E., & Kolattukudy, P. E. (1979). Composition of the aliphatic components of "suberin" from the bundle sheaths of *Zea mays* leaves. *Plant Science Letters*, *15*, 225–230. https://doi.org/10.1016/0304-4211(79)90114-7

Evert, R. F. (2006). Epidermis. *Esau's Plant Anatomy*, 211–253.

Fernández, V., Bahamonde, H. A., Peguero-Pina, J. J., Gil-Pelegrín, E., Sancho-Knapik, D., Gil, L., Goldbach, H. E., & Eichert, T. (2017). Physico-chemical properties of plant cuticles and their functional and ecological significance. *Journal of Experimental Botany*, *68*, 5293–5306. https://doi.org/10.1093/jxb/erx302

Fernández, V., Guzmán-Delgado, P., Graça, J., Santos, S., & Gil, L. (2016). Cuticle structure in relation to chemical composition: Re-assessing the prevailing model. *Frontiers in Plant Science*, *7*, 1–14. https://doi.org/10.3389/fpls.2016.00427

Fernández, V., Sancho-Knapik, D., Guzmán, P., Peguero-Pina, J. J., Gil, L., Karabourniotis, G., Khayet, M., Fasseas, C., Heredia-Guerrero, J. A., Heredia, A., & Gil-Pelegrín, E. (2014). Wettability, polarity, and water absorption of holm oak leaves: Effect of leaf side and age. *Plant Physiology*, *166*, 168–180. https://doi.org/10.1104/pp.114.242040

Fich, E. A., Segerson, N. A., & Rose, J. K. C. (2016). The plant polyester cutin: Biosynthesis, structure, and biological roles. *Annual Review of Plant Biology*, *67*, 18.1-18.27. https://doi.org/10.1146/annurev-arplant-043015-111929

Gao, L., Yang, G., Li, Y., Fan, N., Li, H., Zhang, M., Xu, R., Zhang, M., Zhao, A., Ni, Z., & Zhang, Y. (2019). Fine mapping and candidate gene analysis of a QTL associated with leaf rolling index on chromosome 4 of maize (*Zea mays L.*). *Theoretical and Applied Genetics*, *132*, 3047–3062. https://doi.org/10.1007/s00122-019-03405-1

Grant, R. F., Jackson, B. S., Kiniry, J. R., & Arkin, G. F. (1989). Water deficit timing effects on yield components in maize. *Agronomy Journal*, *81*, 61–65. https://doi.org/10.2134/agronj1989.00021962008100010011x

Griffith, M., Huner, N. P. A., Espelie, K. E., & Kolattukudy, P. E. (1985). Lipid polymers accumulate in the epidermis and mestome sheath cell walls during low temperature development of winter rye leaves. *Protoplasma*, *125*, 53–64. https://doi.org/10.1007/BF01297350

Hansey, C. N., Johnson, J. M., Sekhon, R. S., Kaeppler, S. M., & de Leon, N. (2011). Genetic diversity of a maize association population with restricted phenology. *Crop Science*, *51*, 704–715. https://doi.org/10.2135/cropsci2010.03.0178

Hegebarth, D., Buschhaus, C., Wu, M., Bird, D., & Jetter, R. (2016). The composition of surface wax on trichomes of *Arabidopsis thaliana* differs from wax on other epidermal cells. *The Plant Journal*, *88*, 762–774.

Hegebarth, D., & Jetter, R. (2017). Cuticular waxes of *Arabidopsis thaliana* shoots: Cell-type-specific composition and biosynthesis. *Plants*, *6*, 1–19. https://doi.org/10.3390/plants6030027

Hoad, S. P., Grace, J., & Jeffree, C. E. (1996). A leaf disc method for measuring cuticular conductance. *Journal of Experimental Botany*, *47*, 431–437. https://doi.org/10.1093/jxb/47.3.431

Hoffmann, L., Besseau, S., Geoffroy, P., Ritzenthaler, C., Meyer, D., Lapierre, C., Pollet, B., & Legrand, M. (2004) Silencing of hydroxycinnamoyl-coenzyme A shikimate/quinate hydroxycinnamoyl-transferase affects phenylpropanoid biosynthesis. *Plant Cell*. *16*,1446.

Hsiao, T. C., Otoole, J. C., Yambao, E. B., & Turner, N. C. (1984). Influence of osmotic adjustment on leaf rolling and tissue death in rice (*Oryza sativa L.*). *Plant Physiology*, *75*, 338–341.

Isaacson, T., Kosma, D. K., Matas, A. J., Buda, G. J., He, Y., Yu, B., Pravitasari, A., Batteas, J. D., Stark, R. E., Jenks, M. A., & Rose, J. K. C. (2009). Cutin deficiency in the tomato fruit cuticle consistently affects resistance to microbial infection and biomechanical properties, but not transpirational water loss. *The Plant Journal*, *60*, 363–377. https://doi.org/10.1111/j.1365-313X.2009.03969.x

Jeffree, C. E. (2006) The fine structure of the plant cuticle. Annu Plant Rev Vol 23 Biol Plant Cuticle. Blackwell Publishing Ltd, pp 11–125.

Jetter, R., Kunst, L., & Samuels, A. L. (2006). Composition of plant cuticular waxes. *Biology of the Plant Cuticle*, *23*, 145–181.

Jetter, R., & Riederer, M. (2016). Localization of the transpiration barrier in the epi- and intracuticular waxes of eight plant species: Water transport resistances are associated with fatty acyl rather than

alicyclic components. *Plant Physiology*, *170*, 921–934. https://doi.org/10.1104/pp.15.01699

Jun, J. H., Song, Z., Liu, Z., Nikolau, B. J., Yeung, E. S., & Lee, Y. J. (2010). High-spatial and high-mass resolution imaging of surface metabolites of *Arabidopsis thaliana* by laser desorption-ionization mass spectrometry using colloidal silver. *Analytical Chemistry*, *82*, 3255–3265.

Kadioglu, A., & Terzi, R. (2007). A dehydration avoidance mechanism: Leaf rolling. *Botanical Review*, *73*, 290–302. https://doi.org/10.1663/0006-8101(2007)73[290:ADAMLR]2.0.CO;2

Kadioglu, A., Terzi, R., Saruhan, N., & Saglam, A. (2012). Current advances in the investigation of leaf rolling caused by biotic and abiotic stress factors. *Plant Science*, *182*, 42–48. https://doi.org/10.1016/j.plantsci.2011.01.013

Kerstiens, G. (1996). Cuticular water permeability and its physiological significance. *Journal of Experimental Botany*, *47*, 1813–1832. https://doi.org/10.1093/jxb/47.12.1813

Kessler, S., Seiki, S., & Sinha, N. (2002). Xcl1 causes delayed oblique periclinal cell divisions in developing maize leaves, leading to cellular differentiation by lineage instead of position. *Development*, *129*, 1859–1869.

Kim, D., Langmead, B., & Salzberg, S. L. (2015). HISAT: A fast spliced aligner with low memory requirements. *Nature Methods*, *12*, 357–360. https://doi.org/10.1038/nmeth.3317

Koch, K., & Ensikat, H. J. (2008). The hydrophobic coatings of plant surfaces: Epicuticular wax crystals and their morphologies, crystallinity and molecular self-assembly. *Micron*, *39*, 759–772. https://doi.org/10.1016/j.micron.2007.11.010

Kosma, D. K., Bourdenx, B., Bernard, A., Parsons, E. P., Lü, S., Joubès, J., & Jenks, M. A. (2009). The impact of water deficiency on leaf cuticle lipids of Arabidopsis. *Plant Physiology*, *151*, 1918–1929. https://doi.org/10.1104/pp.109.141911

Kosma, D. K., Molina, I., Ohlrogge, J. B., & Pollard, M. (2012). Identification of an Arabidopsis Fatty Alcohol:Caffeoyl-Coenzyme A Acyltransferase Required for the Synthesis of Alkyl Hydroxycinnamates in Root Waxes. *Plant Physiology*, *160*(1), 237–248. https://doi.org/10.1104/pp.112.201822

Krauss, P., Markstädter, C., & Riederer, M. (1997). Attenuation of UV radiation by plant cuticles from woody species. *Plant, Cell and Environment*, *20*, 1079–1085. https://doi.org/10.1111/j.1365-3040.1997.tb00684.x

Kurdyukov, S., Faust, A., Nawrath, C., Bär, S., Voisin, D., Efremova, N., Franke, R., Schreiber, L., Saedler, H., Métraux, J.-P., & Yephremov, A. (2006). The epidermis-specific extracellular BODYGUARD controls cuticle development and morphogenesis in Arabidopsis. *The Plant Cell*, *18*, 321–339.

Leide, J., Hildebrandt, U., Reussing, K., Riederer, M., & Vogg, G. (2007) The developmental pattern of tomato fruit wax accumulation and its impact on cuticular transpiration barrier properties: Effects of a deficiency in a β-Ketoacyl-Coenzyme A synthase (LeCER6). *Plant Physiology*, *144*, 1667–1679.

Li-Beisson, Y., Pollard, M., Sauveplane, V., Pinot, F., Ohlrogge, J., & Beisson, F. (2009). Nanoridges that characterize the surface morphology of flowers require the synthesis of cutin polyester. *Proceedings of the National Academy of Sciences of the United States of America*, *106*(51), 22008–22013. https://doi.org/10.1073/pnas.0909090106

Lin, M., Matschi, S., Vasquez, M., Chamness, J., Kaczmar, N., Baseggio, M., Miller, M., Stewart, E. L., Qiao, P., Scanlon, M. J., Molina, I., Smith, L. G., & Gore, M. A. (2020). Genome-wide association study for maize leaf cuticular conductance identifies candidate genes involved in the regulation of cuticle development. *G3 Genes|genomes|genetics*, *10*, 1671–1683. https://doi.org/10.1534/g3.119.400884

Luo, A., Rasmussen, C., Hoyt, C., & Sylvester, A. (2013). Warty2 encodes a putative receptor-like Tyr kinase that contributes to maize leaf blade cell expansion. Maize Genet Conf Abstr., p54:T24.

Mazurek, S., Garroum, I., Daraspe, J., De Bellis, D., Olsson, V., Mucciolo, A., Butenko, M. A., Humbel, B. M., & Nawrath, C. (2017). Connecting the molecular structure of cutin to ultrastructure and physical properties of the cuticle in petals of Arabidopsis. *Plant Physiology*, *173*, 1146–1163. https://doi.org/10.1104/pp.16.01637

Mazurek, S., Mucciolo, A., Humbel, B. M., & Nawrath, C. (2013). Transmission Fourier transform infrared microspectroscopy allows simultaneous assessment of cutin and cell-wall polysaccharides of Arabidopsis petals. *The Plant Journal*, *74*, 880–891. https://doi.org/10.1111/tpj.12164

Molina, I., & Kosma, D. (2015). Role of HXXXD-motif/BAHD acyltransferases in the biosynthesis of extracellular lipids. *Plant Cell Reports*, *34*, 587–601. https://doi.org/10.1007/s00299-014-1721-5

Moulia, B. (1994). The biomechanics of leaf rolling. *Biomimetics*, *2*, 267–281.

Moulia, B. (2000). Leaves as shell structures: Double curvature, auto-stresses, and minimal mechanical energy constraints on leaf rolling in grasses. *Journal of Plant Growth Regulation*, *19*, 19–30. https://doi.org/10.1007/s003440000004

Nelson, J. M., Lane, B., & Freeling, M. (2002). Expression of a mutant maize gene in the ventral leaf epidermis is sufficient to signal a switch of the leaf's dorsoventral axis. *Development*, *129*, 4581–4589.

O'Toole, J. C., & Cruz, R. T. (1980). Response of leaf water potential, stomatal resistance, and leaf rolling to water stress. *Plant Physiology*, *65*, 428–432. https://doi.org/10.1104/pp.65.3.428

O'Toole, J. C., Cruz, R. T., & Singh, T. N. (1979). Leaf rolling and transpiration. *Plant Science Letters*, *16*, 111–114. https://doi.org/10.1016/0304-4211(79)90015-4

Poethig, R. S. (1990). Phase change and the regulation of shoot morphogenesis in plants. *Science*, *250*, 923–930. https://doi.org/10.1126/science.250.4983.923

Pollard, M., Beisson, F., Li, Y., & Ohlrogge, J. B. (2008). Building lipid barriers: Biosynthesis of cutin and suberin. *Trends in Plant Science*, *13*, 236–246. https://doi.org/10.1016/j.tplants.2008.03.003

Qiao, P., Lin, M., Vasquez, M., Matschi, S., Chamness, J., Baseggio, M., Smith, L. G., Sabuncu, M. R., Gore, M. A., & Scanlon, M. J. (2019). Machine learning enables high-throughput phenotyping for analyses of the genetic architecture of bulliform cell patterning in maize. *G3 Genes|genomes|genetics*, *9*, 4235–4243. https://doi.org/10.1534/g3.119.400757

Rautengarten, C., Ebert, B., Ouellet, M., Nafisi, M., Baidoo, E. E. K., Benke, P., Stranne, M., Mukhopadhyay, A., Keasling, J. D., Sakuragi, Y., Scheller, H. V. (2012). Arabidopsis *Deficient in Cutin Ferulate* encodes a transferase required for feruloylation of ω-hydroxy fatty acids in cutin polyester. *Plant Physiology*, *158*, 654–665.

Redmann, R. E. (1985). Adaptation of grasses to water stress - leaf rolling and stomate distribution. *Annals of the Missouri Botanical Garden*, *72*, 833. https://doi.org/10.2307/2399225

Reynolds, J., Eisses, J., & Sylvester, A. (1998). Balancing division and expansion during maize leaf morphogenesis: Analysis of the mutant, warty-1. *Development*, *125*, 259–268.

Riederer, M., & Schönherr, J. (1988). Development of plant cuticles: Fine structure and cutin composition of *Clivia miniata Reg*. leaves. *Planta*, *174*, 127–138. https://doi.org/10.1007/BF00394885

Riederer, M., & Schreiber, L. (1995). Waxes - The transport barriers of plant cuticles. *Waxes: Chemistry, Molecular Biology and Functions*, 130–156.

Riederer, M., & Schreiber, L. (2001). Protecting against water loss: Analysis of the barrier properties of plant cuticles. *Journal of Experimental Botany*, *52*, 2023–2032. https://doi.org/10.1093/jexbot/52.363.2023

Ristic, Z., Jenks, M. A. (2002). Leaf cuticle and water loss in maize lines differing in dehydration avoidance. *Journal of Plant Physiology*, *159*, 645–651. https://doi.org/10.1078/0176-1617-0743

Sadler, C., Schroll, B., Zeisler, V., Waßmann, F., Franke, R., & Schreiber, L. (2016). Wax and cutin mutants of Arabidopsis: Quantitative

characterization of the cuticular transport barrier in relation to chemical composition. *Molecular and Cell Biology of Lipids*, *1861*, 1336–1344. https://doi.org/10.1016/j.bbalip.2016.03.002

Saglam, A., Kadioglu, A., Demiralay, M., & Terzi, R. (2014). Leaf rolling reduces photosynthetic loss in maize under severe drought. *Acta Botanica Croatica*, *73*, 315–332. https://doi.org/10.2478/botcro-2014-0012

Schönherr, J. (1976). Water permeability of isolated cuticular membranes: The effect of cuticular waxes on diffusion of water. *Planta*, *131*, 159–164. https://doi.org/10.1007/BF00389989

Schreiber, L. (2005). Polar paths of diffusion across plant cuticles: New evidence for an old hypothesis. *Annals of Botany*, *95*, 1069–1073. https://doi.org/10.1093/aob/mci122

Serrano, M., Coluccia, F., Torres, M., L'Haridon, F., & Métraux, J.-P. (2014). The cuticle and plant defense to pathogens. *Frontiers in Plant Science*, *5*, 274. https://doi.org/10.3389/fpls.2014.00274

Shields, L. M. (1951). The involution mechanism in leaves of certain xeric grasses. *Phytomorphology*, *1*, 225–241.

Sylvester, A. W., & Smith, L. G. (2009). Cell biology of maize leaf development. In J. L. Bennetzen, & S. C. Hake (Eds.), *Handb Maize Its Biol* (pp. 179–203). Springer.

Turner, N. C., O'Toole, J. C., Cruz, R. T., Namuco, O. S., & Ahmad, S. (1986). Responses of seven diverse rice cultivars to water deficits I. Stress development, canopy temperature, leaf rolling and growth. *Field Crops Research*, *13*, 257–271. https://doi.org/10.1016/0378-4290(86)90027-4

Veličkovic, D., Herdier, H., Philippe, G., Marion, D., Rogniaux, H., & Bakan, B. (2014). Matrix-assisted laser desorption/ionization mass spectrometry imaging: A powerful tool for probing the molecular topology of plant cutin polymer. *The Plant Journal*, *80*, 926–935. https://doi.org/10.1111/tpj.12689

Weissflog, I., Vogler, N., Akimov, D., Dellith, A., Schachtschabel, D., Svatos, A., Boland, W., Dietzek, B., & Popp, J. (2010). Toward *in vivo* chemical imaging of epicuticular waxes. *Plant Physiology*, *154*, 604–610. https://doi.org/10.1104/pp.110.161786

Willick, I. R., Lahlali, R., Vijayan, P., Muir, D., Karunakaran, C., & Tanino, K. K. (2018). Wheat flag leaf epicuticular wax morphology and composition in response to moderate drought stress are revealed by SEM, FTIR-ATR and synchrotron X-ray spectroscopy. *Physiologia Plantarum*, *162*, 316–332. https://doi.org/10.1111/ppl.12637

Xiao, F., Goodwin, S. M., Xiao, Y., Sun, Z., Baker, D., Tang, X., Jenks, M. A., & Zhou, J.-M. (2004). Arabidopsis CYP86A2 represses *Pseudomonas syringae* type III genes and is required for cuticle development. *The EMBO Journal*, *23*, 2903–2913. https://doi.org/10.1038/sj.emboj.7600290

Xu, P., Ali, A., Han, B., & Wu, X. (2018). Current advances in molecular basis and mechanisms regulating leaf morphology in rice. *Frontiers in Plant Science*, *9*, 1528. https://doi.org/10.3389/fpls.2018.01528

Yeats, T. H., & Rose, J. K. C. (2013). The formation and function of plant cuticles. *Plant Physiology*, *163*, 5–20. https://doi.org/10.1104/pp.113.222737

Yu, M. M. L., Konorov, S. O., Schulze, H. G., Blades, M. W., Turner, R. F. B., & Jetter, R. (2008). *In situ* analysis by microspectroscopy reveals triterpenoid compositional patterns within leaf cuticles of *Prunus laurocerasus*. *Planta*, *227*, 823–834. https://doi.org/10.1007/s00425-007-0659-z

Zou, L., Zhang, Z., Qi, D., Peng, M., & Lu, T. (2014). Cytological mechanisms of leaf rolling in rice. *Crop Science*, *54*, 198–209. https://doi.org/10.2135/cropsci2013.03.0199

SUPPORTING INFORMATION

Additional Supporting Information may be found online in the Supporting Information section.

How to cite this article: Matschi S, Vasquez MF, Bourgault R, et al. Structure-function analysis of the maize bulliform cell cuticle and its potential role in dehydration and leaf rolling. *Plant Direct*. 2020;00:1–21. https://doi.org/10.1002/pld3.282